22

Plasma Interaction of Io with its Plasma Torus

Joachim Saur
Dept. of Earth and Planetary Sciences, The Johns Hopkins University

Fritz M. Neubauer
Institut für Geophysik und Meteorologie, Universität zu Köln

J. E. P. Connerney
NASA Goddard Space Flight Center

Philippe Zarka
Observatoire de Paris, Meudon

Margaret G. Kivelson
IGPP and Dept. of Earth & Space Sciences, University of California, Los Angeles

22.1 INTRODUCTION AND HISTORY

Io's plasma interaction with its torus is an exceptionally interesting case of magnetospheric plasma flowing past a body with a tenuous atmosphere. Major progress in our understanding of Io's interaction has occurred in the last 10 years based on the rich data sets acquired by the *Galileo* spacecraft in orbit around Jupiter with seven close flybys of Io supplemented by Earth-based remote-sensing observations of unprecedented resolution. This system, i.e., Io and its atmosphere, the Io plasma torus, and Jupiter with its magnetosphere, is very strongly coupled with a number of feedback mechanisms. In the history of space science, this system has also played an important role in the progress of understanding satellite plasma interactions in general.

Our first aim with this chapter is to explain the basic physical mechanisms of Io's plasma interaction. For simplicity, we divide Io's interaction into its *local interaction* and its *far-field interaction* although both are strongly coupled. The local interaction occurs within a few satellite radii of Io, which thus comprises Io's atmosphere, ionosphere and corona. The far-field interaction region includes Io's plasma torus, Jupiter's ionosphere and the high magnetospheric latitudes (i.e., just above Jupiter's ionosphere, where the plasma is very dilute). Our second aim is to present the major findings at this current epoch of the *Galileo* spacecraft and Earth-based observations and to relate them to the physical mechanisms of the interaction.

This chapter is closely related to Chapter 21 where the electrodynamic interactions at the Galilean satellites in general are presented. We also point to Hill *et al.* (1983), which reviews the subject of Io's plasma interaction.

We develop this chapter in the following way. As a general orientation for a reader new to the subject, we first introduce the basics of Io's plasma interaction. With this background, we present a short history of salient observational and theoretical findings through the early nineties. In Section 22.2, we review the fundamental theoretical concepts of Io's local and far-field interactions and their feedback mechanisms. In Section 22.3 we discuss recent observations of the local interaction close to Io by the *Galileo* spacecraft and relevant Earth-based observations. These observations are the major motivation of this chapter and are discussed in the context of the former theory. In Section 22.4 we present observations of the far-field interaction and interpret them in terms of the physics of Io's interaction. We end with a brief Section 22.5 that identifies remaining unresolved questions.

22.1.1 The Basics of Interaction

The most important elements that make Io's electrodynamic interaction unique in our solar system are Jupiter's strong magnetic field, its fast rotation, and Io's volcanism. The strong magnetic field of Jupiter creates the largest magnetosphere in our solar system. Thus Io and the other Galilean moons are always deep within Jupiter's magnetosphere. In contrast, for example, Earth's moon passes through the tail of Earth's magnetosphere once per month. Therefore the Io interaction is qualitatively different from that of comets, planets or other bodies, which are exposed to the solar wind (see Chapter 21). Io is also the most volcanically active body in our solar system (see Chapter 14) with more than 100 known active volcanoes. These volcanoes create, along with sublimation of surface frosts, a tenuous and patchy atmosphere on Io (see Chapter 19) that is thought to consist mainly of SO_2. Through several processes, Io's atmosphere loses matter into the jovian magnetosphere where the mass arrives in part ionized and in part neutral. The neutrals are

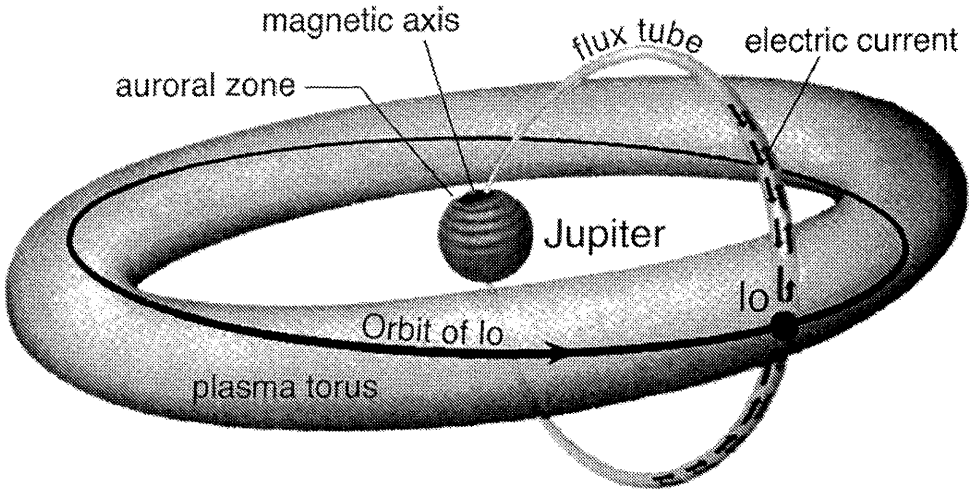

Figure 22.1. Sketch of the Io plasma torus and the general geometrical setup, after Audouze *et al.* 1988.

then ionized by UV radiation or electron impact ionization. The new ions and electrons accumulate around the orbit of Io and form the Io plasma torus shown in Figure 22.1. The total mass loss rate from Io, which maintains the torus, is thought to be about one ton per second (Chapter 23).

The new plasma is subject to electrodynamic forces that accelerate it to the local bulk plasma velocity. Upstream of Io the plasma nearly fully corotates with Jupiter, i.e., has the same angular velocity as Jupiter. The plasma of the torus consists mostly of the ions of SO_2, i.e., S^+, S^{++}, O^+, O^{++}, etc., which eventually populate the whole magnetosphere of Jupiter. Therefore the plasma of the jovian magnetosphere, in contrast to that of Earth, contains mostly heavy ions.

Io orbits Jupiter with a velocity of 17 km s^{-1}. Jupiter's rotation period of about 10 hours makes the Io plasma torus rotate with a velocity of about 74 km s^{-1}. Since Io is embedded in the Io plasma torus, the torus plasma flows past Io with a relative velocity of 57 km s^{-1}. One can also say Io is being constantly overtaken by its own tail, one rotation period later, because the plasma originates from Io.

This flow of magnetized plasma past the obstacle Io, with its tenuous atmosphere, is the engine of Io's plasma interaction. There are two reasons why the plasma is perturbed at Io: (1) The plasma density, momentum, and energy is modified through elastic and inelastic collisions with Io's atmosphere and photoionization; (2) The solid body of Io absorbs plasma that is advected on to the surface. These processes produce a very intense electrodynamic interaction, with an electric current system of a total of about 10 million amperes that has immense consequences locally, but which also extends far away towards Jupiter, particularly in the direction of the magnetic field (see Figure 22.1 for a simplified picture). This interaction is also related to the footprints of Io that can be seen in Jupiter's upper atmosphere (see Section 22.4.1), and it also controls part of the radio emission that is emitted from the jovian magnetosphere (see Section 22.4.2). The auroral emissions associated with the Io–Jupiter interaction are further discussed in Chapter 26.

22.1.2 History

With this background, we now briefly review the most important observations and theoretical concepts that have been developed for Io's interaction.

From the Discovery of the Io Effect to Mid-1990

The discovery of the Io effect, i.e., Io's statistical control over Jupiter's decametric radiation, by Bigg (1964) gave the first evidence for a strong electrodynamic interaction between Io and the jovian magnetosphere and thereby initiated the research on Io's plasma interaction. The next big step came with the first spacecraft, *Pioneer 10* and *Pioneer 11*, that visited the Jupiter system in 1973/74. The detection of an ionosphere by *Pioneer 10* (Kliore *et al.* 1975) and the Earth-based observations of neutral clouds of sodium in the vicinity of Io by Brown and Chaffee (1974) (see Chapter 23) related the electrodynamic interaction to a neutral atmosphere on Io. Another major observational building block for Io's interaction was found by the *Voyager 1* and *Voyager 2* Jupiter flybys in 1979. Broadfoot *et al.* (1979) and Bridge *et al.* (1979) identified the dense, luminous plasma known as the Io plasma torus. Previous hints had already existed from observations of ionized sulfur lines in the inner magnetosphere around Io by Kupo *et al.* (1976). Several authors had also postulated that the *Pioneer 10* plasma and UV observations, initially interpreted in terms of enhanced density of light ions, actually represented heavy ions (see reviews in Belcher (1983) and Brown *et al.* (1983)). *Voyager 1* also discovered that Io has the most active volcanism in the solar system (Smith *et al.* 1979, Morabito *et al.* 1979), driven probably by orbital resonance with Europa and Ganymede, as predicted by Peale *et al.* (1979) just prior to the actual observation. The *Voyager* IRIS experiment first detected directly a localized volcanic plume atmosphere of SO_2 (Pearl *et al.* 1979). The Io plasma torus composition provided additional evidence for SO_2 as the dominant atmospheric species (Bridge *et al.* 1979). More than 10 years had to pass until the first Earth-based detection of Io's SO_2 atmosphere by Lellouch *et al.* (1990). Direct evidence for the strong electrody-

namic interaction came from the magnetic field observations of the *Voyager* spacecraft (Ness *et al.* 1979), which inferred an estimated electric current in Io's flux tube/Alfvén wings of 2.8×10^6 ampere (Acuña *et al.* 1981). Additional recent evidence for a powerful electrodynamic interaction are the observations of near-IR and UV radiation at the footprints of the Io flux tube intersecting Jupiter's auroral atmosphere (Connerney *et al.* 1993, Clarke *et al.* 1996, Prangé *et al.* 1996).

Theoretical progress in identifying the underlying mechanisms was closely linked to the observational progress. The first theoretical model of the electrodynamic interaction between Io and Jupiter was the unipolar inductor model of Piddington and Drake (1968), which was substantially modified by Goldreich and Lynden-Bell (1969), at a time when the existence of Io's atmosphere and plasma torus were not observationally established. This model was developed to explain Io's control of decametric emission from Jupiter. Motivated by the discovery of Io's ionosphere, Cloutier *et al.* (1978) created one of the first models of Io's local interaction and pointed out that Io's ionosphere is not in Earth-like chemical equilibrium, but strongly advection-dominated. After the discovery of the dense Io plasma torus, a paradigm change occurred and the interaction was more appropriately described in terms of magneto-hydrodynamic (MHD) wave modes. In particular, the Alfvén mode plays the essential role for carrying approximately field-aligned electric current. Starting from the linear Alfvén wave model of Drell *et al.* (1965), Neubauer (1980) provided a general analytical solution for the nonlinear standing Alfvénic current system together with a solution for a simplified Alfvén tube. Goertz (1980) also considered an Alfvénic interaction, but focused on the local interaction with a pickup model for the closure currents and on radiation properties of the Alfvén waves in the torus. Additional aspects on the Alfvénic interaction, such as the wake structure, were considered by Southwood *et al.* (1980) and Southwood and Dunlop (1984).

The Current Epoch: Galileo, HST and Earth-Based Telescopes

The observations obtained by the *Galileo* spacecraft, in orbit around Jupiter since December 1995, marked a new milestone in our knowledge of Io's interaction. The *Galileo* spacecraft made seven close Io flybys during its mission which yielded a wealth of spectacularly interesting data. Further observational progress was made during the last 10 years from Earth-based remote sensing measurements. In the remainder of this chapter we will first present the theoretical basis of the Io–plasma interaction, followed by the observations and their interpretation.

22.2 THEORETICAL CONCEPTS OF THE IO–PLASMA INTERACTION

As sketched in Section 22.1.1, Io's interaction is generated locally at Io but extends out into Jupiter's magnetosphere. For simplicity we divide Io's interaction into two different regions, which we describe separately, although they are actually strongly coupled: the *local interaction* region, which includes Io and extends only a few Io radii; and the *far-field interaction* region, which includes Jupiter and the inner jovian magnetosphere.

22.2.1 Approaches to Modeling: Dimensionless Parameters

For the given upstream plasma conditions at Io (see Chapter 21) there is more energy in the magnetic field than in the bulk velocity or the thermal velocity. This is equivalently reflected in the low Alfvén Mach number $M_A^2 = 0.09$ (with M_A the ratio of bulk flow velocity to the Alfvén velocity) and the low plasma beta $\beta = 0.04$ (where β is the ratio of thermal pressure to magnetic field pressure; see Chapter 21 for further discussion). Thus the stiffness of the strong background magnetic field of Jupiter plays the dominant role in determining the topology of the interaction and makes the interaction essentially anisotropic.

Another important characteristic parameter at Io is the sonic Mach number, which is larger than one. The sonic and the Alfvén Mach numbers determine the fast Mach number, which is smaller than one and thus no bow shock forms at Io. This is a strong qualitative constraint on Io's interaction.

Before we present a physical model for Io's plasma interaction, we examine the question of the appropriate physical framework to describe Io's interaction. Chapter 21 shows that the typical microscopic lengths and timescales, such as ion gyroradius and gyroperiods, are small compared to the global scales of Io, i.e., its radius, atmospheric scale heights etc., and flow times, respectively. This allows us to use a fluid approach to describe Io's large-scale plasma interaction. Plasma densities are large enough so that the Debye lengths are small compared to the typical length scale, ensuring quasi-neutrality. There are, however, also important effects that take place on smaller scales that cannot be accounted for in a fluid framework and where kinetic approaches are required (see Section 22.3.2).

22.2.2 Fluid Equations

The most general fluid approach is a multi-fluid description that takes into account an electron fluid and a host of ion fluids. The appropriate set of equations has been given frequently in the literature (e.g., Schunk (1975), Banks and Kockarts (1973a), Banks and Kockarts (1973b), or Neubauer (1998b)). These are equations for mass density, momentum, and energy, and Maxwell's equations. This set of equations can be further adapted or simplified for (a) the local interaction region, i.e., Io's ionosphere, and the far-field interaction region, which we subdivide into (b1) the Io plasma torus, and (b2) the high latitude regions of Jupiter's magnetosphere.

(a) A Multi-Fluid Description for Io's Ionosphere

In Io's atmosphere a multi-fluid approach is required since aeronomic processes need to be taken into account. The approach should include the complex chemical interactions among the atmospheric and ionospheric species, like SO_2, SO, O, SO_2^+, together with different ionization processes such as electron impact ionization and photoionization, and

the appropriate momentum transfer processes such as elastic collisions, charge exchange, etc., and energy transfer processes such as cooling mechanisms, heat conduction, etc. For simplicity, we will outline this approach with a two-fluid model comprising one ion fluid (representing all ion species) and an electron fluid.

Continuity equation. The evolution of the plasma density n is given by

$$\frac{\partial n}{\partial t} + \nabla \cdot (n\boldsymbol{v}) = P - L \tag{22.1}$$

with the production rate P and the loss rate L. For quasi-neutrality the singly charged ion particle density n_i equals the electron particle density n_e.

Momentum equations. What we called earlier the engine of Io's interaction is momentum exchange of the plasma with Io's atmosphere. Its effect is generally to slow down the incoming plasma and to accelerate Io's neutral atmosphere. The momentum exchange happens via elastic collisions described by the ion/electron-neutral collision frequencies, ν_in and ν_en, (which includes charge exchange for the ions) and via mass loading P, i.e., the pickup processes. Their effects can be combined in effective collision frequencies (Neubauer 1998b)

$$\tilde{\nu}_\mathrm{in} = \nu_\mathrm{in} + P/n_\mathrm{i} \quad \text{and} \quad \tilde{\nu}_\mathrm{en} = \nu_\mathrm{en} + P/n_\mathrm{e} \tag{22.2}$$

The velocity equation for the electrons and the ions (e.g., Schunk (1975), Neubauer (1998b), Szegö *et al.* (2000)) can be expressed as an equation for the bulk plasma flow $\boldsymbol{v} = (\rho_\mathrm{i}\boldsymbol{v}_\mathrm{i} + \rho_\mathrm{e}\boldsymbol{v}_\mathrm{e})/(\rho_\mathrm{i} + \rho_\mathrm{e})$ and as an Ohm's law for the electric current $\boldsymbol{j} = e(n_\mathrm{i}\boldsymbol{v}_\mathrm{i} - n_\mathrm{e}\boldsymbol{v}_\mathrm{e})$, both of which include the momentum exchange with the atmosphere (m_i, m_e, particle mass; ρ_i, ρ_e, mass density; $\boldsymbol{v}_\mathrm{i}$, $\boldsymbol{v}_\mathrm{e}$; velocity; p_i, p_e; pressure of the ions and electrons, respectively, and e, elementary charge). We will write these equations assumpting $m_\mathrm{e}/m_\mathrm{i} \ll 1$ and neglecting terms of the form $\propto j^2$, and $\propto vj$. The evolution equation for the bulk velocity is calculated by adding electron and ion velocity equations (e.g., Equations (11) and (12) in Neubauer (1998b) multiplied by the appropriate mass density and without ion–electron collisions)

$$\rho\frac{\mathrm{d}}{\mathrm{d}t}\boldsymbol{v} = -\nabla p + \boldsymbol{j}\times\boldsymbol{B} + n(m_\mathrm{i}\tilde{\nu}_\mathrm{in} + m_\mathrm{e}\tilde{\nu}_\mathrm{en})(\boldsymbol{v_\mathrm{n}} - \boldsymbol{v}) + (\tilde{\nu}_\mathrm{en} - \tilde{\nu}_\mathrm{in})\frac{m_\mathrm{e}}{e}\boldsymbol{j} \tag{22.3}$$

where B is the magnetic field, $\rho = \rho_\mathrm{i} + \rho_\mathrm{e}$ and $p = p_\mathrm{i} + p_\mathrm{e}$ define total mass density and total plasma pressure, respectively. The last two terms on the right hand describe the action of Io's atmosphere on the plasma via collisions and mass loading. Ohm's law is derived by subtracting the same electron velocity equation from the ion velocity equation in combination with (22.1)

$$\frac{\mathrm{d}}{\mathrm{d}t}\boldsymbol{j} = e\nabla\left(\frac{p_\mathrm{e}}{m_\mathrm{e}} - \frac{p_\mathrm{i}}{m_\mathrm{i}}\right) + \frac{e}{m_\mathrm{e}}(en(\boldsymbol{E} + \boldsymbol{v}\times\boldsymbol{B}) - \boldsymbol{j}\times\boldsymbol{B}) + en(\nu_\mathrm{in} - \nu_\mathrm{en})(\boldsymbol{v}_\mathrm{n} - \boldsymbol{v}) - \boldsymbol{j}\left(\frac{L}{n} + \nu_\mathrm{en} + \frac{m_\mathrm{e}}{m_\mathrm{i}}\nu_\mathrm{in}\right) \tag{22.4}$$

where $\mathbf{E}$ is the electric field. The first thing to notice is that the frozen-in field theorem, $\boldsymbol{E} = -\boldsymbol{v}\times\boldsymbol{B}$ (concomitant with ideal MHD), does not hold, particularly in the ionosphere where collisional terms are important. Note, that in the bulk velocity equation the loss rate L does not appear, since taking a plasma particle out of an arbitrary volume element does not change the velocity, but only the momentum of the volume element. However, the production term is important, and in our description it is embedded in the effective collision frequencies, denoted by a tilde. In Ohm's law, it is formally the opposite. Only the loss term L appears, but the production rate appears implicitly through its dependence on $\boldsymbol{v}$. The loss rate L could also be removed by using (22.1) again.

Energy equations. In addition to the momentum equation, an energy equation for the electrons and ions is required. For brevity, we discuss the most important physics in words.

The electron temperature distribution around Io strongly reflects the anisotropic nature of Io's interaction. While the electron heat conductivity along the magnetic field lines is extremely high in a hot and dilute plasma, it is very small perpendicular to the field lines as long as the neutral density is not so high that electron neutral collisions start to destroy the anisotropy of the conductivity. Electron energy from the Io plasma torus can be transported very efficiently along the magnetic field into Io's ionosphere. This is very important to maintain an ionospheric electron temperature high enough to allow for continued ionization. The high heat conductivity tends to establish a constant temperature along the magnetic field lines, while electrons on different field lines can easily have very different temperatures. Thus the magnetic field configuration close to Io also strongly determines the electron temperature distribution and thus also Io's atmospheric radiation which is excited by electron impact (see Section 22.3.3). A detailed model for the electron temperature at Io can be found for example in Saur *et al.* (1999, 2002).

The ion temperature in Io's ionosphere is predominantly controlled by the interaction with the neutral atmosphere. Ions that are created in the ionosphere acquire a gyration velocity that is given by the local plasma velocity relative to Io's atmosphere. Ion–neutral collisions act in principle in the same way. Collisions reset the ion gyration velocity to the local plasma flow velocity relative to the neutral atmosphere (see e.g., Banks and Kockarts (1973b) or Saur *et al.* (1999)). A full model of Io's total plasma temperature and a discussion of the effects due to mass loading was first given by Linker *et al.* (1989) and used again in Linker *et al.* (1998) and Combi *et al.* (1998), albeit without the effect of electronic heat conduction and electron cooling.

Maxwell's equations. The fluid equations need to be solved together with Maxwell's equations. They include Ampère's law

$$\boldsymbol{\nabla}\times\boldsymbol{B} = \mu_0\boldsymbol{j} + \mu_0\epsilon_0\frac{\partial}{\partial t}\boldsymbol{E} \tag{22.5}$$

with μ_0 and ϵ_0 the magnetic and electric permeability of space, respectively (where Maxwell's displacement current can be neglected in the ionosphere), Faraday's induction equation

$$\frac{\partial}{\partial t}\boldsymbol{B} = -\boldsymbol{\nabla}\times\boldsymbol{E} \tag{22.6}$$

and the solenoidal condition for the magnetic field. Coulomb's equation cannot be used in the fluid approach for the long timescales under consideration (Chen 1984, Green 2000).

(b1) The Io Plasma Torus: Ideal MHD

When considering electrodynamics in the Io torus, the physical effects of the neutral density are unimportant and the collision frequencies and sources and sinks in the set of equations (22.1) to (22.4) can be neglected to first order. If Maxwell's displacement current, the Hall term in Ohm's law, and terms $\propto m_e$ are neglected, equations (22.1) to (22.6) reduce to the standard ideal MHD model, where the frozen-in field theorem applies. The special structure of the MHD equations allows a solution of the nonlinear problem (Neubauer 1980) in this case.

(b2) High Latitudes: Maxwell's Displacement Current and Kinetic Effects

At high magnetic latitudes, i.e., far away from Io and above Jupiter's ionosphere, one can expect, in addition to a negligible neutral density, very low plasma densities. Thus the Alfvén speed approaches the speed of light and Maxwell's displacement current is no longer negligible in (22.5) as it is in standard MHD. Also processes on smaller length scales including electron inertia and kinetic effects become important (e.g., Crary 1997, Delamere *et al.* 2003, Su *et al.* 2002). The physics of the far-field interaction will be discussed in detail in Section 22.2.4.

The B, v and the E, j Approach

Within the MHD approach to magnetized plasmas, there exist two major approaches, the B,v picture and the E,j picture (for example Parker (1996) or Green (2000) and references therein). There is however a longstanding debate: which of these approaches are more appropriate or fundamental to describe a plasma? In the case of Io's interaction, both frameworks have been successfully applied to describe different aspects of the interaction with different levels of precision. In this chapter, we will apply both concepts to explain the physics of Io's interaction. The differences lie in the treatments and assumptions put into equations (22.3) to (22.6). These differences will be elucidated in the rest of this chapter.

22.2.3 The Local Interaction

A Sketch of the Local Interaction

In Figure 22.2 we sketch Io's local interaction. Plasma from the torus streams into Io's atmosphere and forms an ionosphere within Io's atmosphere by electron impact ionization and, to a lesser extent, by photoionization. We now use the E,j picture, and the frozen-in field approximation in Jupiter's magnetosphere, requiring the electric field in the rest frame of the magnetospheric plasma to be zero. Thus an observer in the rest frame of Io sees a motional electric field $\boldsymbol{E_0} = -\boldsymbol{v_0} \times \boldsymbol{B_0}$ with $\boldsymbol{v_0}$ the relative velocity of the unperturbed incident torus plasma, and $\boldsymbol{B_0}$ the background magnetic field at Io. Whereas the plasma has a very high

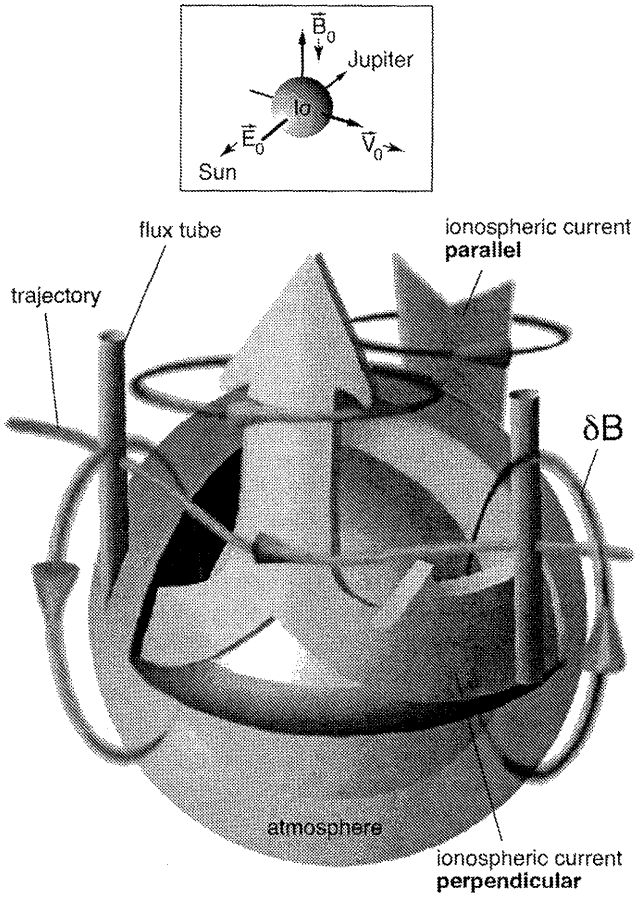

Figure 22.2. Sketch of Io's local interaction with the ionospheric current system and its magnetic field perturbation.

conductivity parallel to the local magnetic field everywhere, in the ionosphere of Io the conductivities perpendicular to the magnetic field become large as well, and thus the motional electric field drives an ionospheric electric current. This current is directed mostly from the Jupiter-facing side of Io to the opposite side (also called the anti-Jupiter side). The ionospheric electric current system shorts out and modifies the electric field by producing polarization charges, i.e., a surplus of positive charges on the anti-Jupiter side and negative charges on the other side. With the modified electric field, the local Lorentz force changes, which modifies in turn the electron and ion flow close to Io. As a result, the plasma flow is strongly reduced and directed around Io. Further away from Io, where the neutral atmosphere becomes thin, the ionospheric conductivities are small and thus cannot maintain the ionospheric current perpendicular to the magnetic field. Then electric current is continued along the magnetic field lines out of Io's ionosphere, where it is finally fed into Io's Alfvén wings (to be discussed in detail in Section 22.2.4). It is important to note that the ultimate energy source for the interaction is not initially in the motional electric field, but in the movement of the magnetized plasma relative to Io, which generates this electric field (for further discussion on the flow and the electric field, see Vasyliūnas 2001).

In the B,v picture the ionospheric and magnetospheric plasma exchange momentum with the neutral atmosphere

via collisions and mass loading. This acts as a force on the plasma and is mostly balanced by the divergence of Maxwell's stress tensor $\nabla \cdot \boldsymbol{M} = -\nabla(B^2/(2\mu_0)) + \nabla \cdot (\boldsymbol{BB})/\mu_0 = \boldsymbol{j} \times \boldsymbol{B}$ (see Eq. (22.3)). In simple words, the magnetic field lines drape around Io. They are slowed in the ionosphere and bend around it (see Figure 22.5 or discussion in Chapter 21). Outside of Io's ionosphere these collisions and mass loading are negligible for the macroscopic dynamics, but the inertia term (left hand side of Equation 22.3) becomes important and establishes mostly the balance with the Maxwell stresses. The local perturbation created in the ionosphere thus immediately starts to propagate. The most important wave mode is the Alfvén mode discussed in more detail in Section 22.2.4.

Models of the Local Interaction

For Io's interaction there are numerous analytic and numerical models. The analytic models will be discussed in the next subsection since they give a good general insight into overall features and dependences of Io's interaction. The physics of the numerical models will be reviewed in this subsection, but we will discuss their results in Section 22.3 since they usually fit the observations in a much more detailed way than do the analytic models.

With the advent of powerful computers, numerical solution to otherwise inaccessible problems became available to describe Io's interaction. In one of the first numerical models, Wolf-Gladrow *et al.* (1987) calculated (in 3D) the electric field, electric current, and magnetic field for given ionospheric densities and conductivities. This is a self-consistent model in the E,j framework using Euler coordinates to adapt to the self-consistently calculated magnetic field geometry. Starting at about the same time, Linker *et al.* (1988, 1989, 1991, 1998) developed a numerical model that solved in the B,v framework for the first time self-consistently, the full set of the one fluid 3-D MHD equations for Io's interaction. This model consequently included the three expected MHD perturbations, i.e., the Alfvén mode, the fast and the slow modes. It solved (22.1) with a prescribed ionization rate, and (22.3) with prescribed collision rates and mass loading. It used an induction equation (22.6) with Ohm's law in (22.4) reduced to $\boldsymbol{E} = -\boldsymbol{v} \times \boldsymbol{B} + \eta \boldsymbol{j}$ (with a prescribed isotropic resistivity η to describe Io's ionosphere, and the terms proportional to m_e and the pressure term neglected). Also in the B,v frame, Combi *et al.* (1998) applied an adaptive multi-scale 3-D numerical model to describe Io's interaction which solves self-consistently the ideal (i.e., no physical resistivity) MHD equations, i.e., (22.4) is $\boldsymbol{E} = -\boldsymbol{v} \times \boldsymbol{B}$. Combi *et al.* (1998) use a prescribed mass loading and drag force (i.e., collision of the plasma with the neutrals) in their velocity equation. Aspects of the interaction have been modeled by Kopp (1996) (with more attention to the far-field and the parallel currents). Saur *et al.* (1999) and Saur *et al.* (2000) approached Io's interaction differently and created a two-fluid plasma model for electrons and one ion species in the E,j framework, which includes self-consistently Io's aeronomic processes, such as different production rates and collision frequencies, but assumes a constant magnetic field. They neglect in (22.3) the inertia and the pressure, maintain in (22.4) the anisotropy, but neglect all terms with spatial and temporal derivatives and terms $\propto m_e$. The results of the numerical models for Io's local interaction will be discussed in detail in Section 22.3 in comparison with the observations.

An Analytic Model of the Local Interaction

In this subsection we present an analytic model which gives good insight into major features of Io's local interaction. Analytic models for Io's local interaction, which are however not self-consistent in the magnetic field, have usually been constructed in the E,j picture. The model here is in the spirit of Goertz (1980), Hill and Pontius (1998), Neubauer (1998b), and Saur *et al.* (1999), Saur (2000). (A classical work by Goldreich and Lynden-Bell (1969) on Io's interaction, which contains also the far-field, is in the E,j picture, too.) The core of these models is an equation for the electric field, which builds the basis for estimates of additional quantities, such as electron and ion velocities, electric currents, and magnetic field perturbations, or plasma densities and temperatures. These models differ in the assumptions about the nature of the far-field interaction (unipolar inductor or Alfvén wing coupling) and the nature of the local interaction (pickup *vs.* ionospheric resistivity). The models are well suited to take advantage of symmetries and invariances of Io's interaction.

Equation for the electric field. In our derivation of the electric field equation we use the following Io-centered coordinate system: The z axis is in the direction opposite to the background magnetic field, the y direction points in direction opposite to the unperturbed motional electric field (i.e., perpendicular to the magnetic field and the flow), the x axis completes the right-handed system and points mainly in direction of the corotational flow. In (22.4) we replace $\boldsymbol{v}$ from (22.3), solve for $\boldsymbol{j}$, and derive another form of the anisotropic Ohm's law

$$\boldsymbol{j} = \sigma_0 \boldsymbol{E}_\parallel + \sigma_1 \boldsymbol{E}_\perp + \sigma_2 \boldsymbol{B} \times \boldsymbol{E}_\perp / B \tag{22.7}$$

in terms of the electric field component $\boldsymbol{E}_\perp$ perpendicular and $\boldsymbol{E}_\parallel$ parallel to the magnetic field as seen in Io's rest frame. Here, the temporal and spatial derivatives of the plasma quantities (velocities, pressures and densities of the electrons and the ions, respectively) are neglected. The parallel conductivity is given by

$$\sigma_0 = \frac{e n_i}{B} \left(\frac{\omega_{ce}}{\tilde{\nu}_{en}} + \frac{\omega_{ci}}{\tilde{\nu}_{in}} \right) \tag{22.8}$$

the Pedersen conductivity by

$$\sigma_1 = \frac{e n_i}{B} \left(\frac{\omega_{ci} \tilde{\nu}_{in}}{\omega_{ci}^2 + \tilde{\nu}_{in}^2} + \frac{\omega_{ce} \tilde{\nu}_{en}}{\omega_{ce}^2 + \tilde{\nu}_{en}^2} \right) \tag{22.9}$$

and the Hall conductivity by

$$\sigma_2 = \frac{e n_i}{B} \left(\frac{\tilde{\nu}_{en}^2}{\omega_{ce}^2 + \tilde{\nu}_{en}^2} - \frac{\tilde{\nu}_{in}^2}{\omega_{ci}^2 + \tilde{\nu}_{in}^2} \right) \tag{22.10}$$

with ω_{ci} and ω_{ce} the ion and electron gyro frequencies, respectively. The electron contribution to the conductivities can be neglected for $\tilde{\nu}_{en} \ll \omega_{ce}$, which is in general a good approximation for Io's atmosphere (Neubauer 1998b). Since we intend to describe the steady-state case, this perpendicular electric current system needs to be continued along the magnetic field for the fundamental reason of charge conservation, i.e., $\nabla \cdot \boldsymbol{j} = 0$. Thus the parallel electric current

arises from the divergence of the perpendicular currents. Currents out of and into Io's ionosphere need to match the currents that are driven in and out of the Alfvén wings ($j_A = \pm\Sigma_A \nabla \cdot \boldsymbol{E}$, where $\Sigma_A = 1/(\mu_0 V_{A_0})$ is the Alfvén conductance with the magnetic permeability μ_0 and the Alfvén velocity V_{A_0} Neubauer 1980). This leads to an equation for the electric field at Io. In addition, we take advantage of the fact that the parallel electric field in Io's ionosphere is negligible, which reduces the electric field to 2D. Here we give this equation written as an equation for the electric potential $\Phi(x, y)$, assuming as a simplifying condition a constant background magnetic field in the z direction

$$(\Sigma_1 + \Sigma_A)\Delta\Phi + \left(\frac{\partial\Sigma_1}{\partial x} - \frac{\partial\Sigma_2}{\partial y}\right)\frac{\partial\Phi}{\partial x} + \left(\frac{\partial\Sigma_1}{\partial y} + \frac{\partial\Sigma_2}{\partial x}\right)\frac{\partial\Phi}{\partial y} = 0 \qquad (22.11)$$

with the boundary condition that the perturbation vanishes at infinity, and the corotational electric field is obtained:

$$\Phi = E_0 y \qquad \sqrt{(x^2 + y^2)} \to \infty \qquad (22.12)$$

With this description the electric field is determined by: (i) the Alfvén conductance Σ_A, and (ii) the contributions of the ionospheric conductivities, included in the conductances by integration along the field lines from the equatorial plane up to and beyond the ionosphere

$$\Sigma_i = \int_{z=0} \mathrm{d}z\, \sigma_i(x, y, z) \qquad i = 1, 2 \qquad (22.13)$$

Note this model assumes that the ionosphere is symmetric with respect to Io's equator. This concept of determining the electric field by taking advantage of given symmetries and thus introduction of height-integrated conductances also has broad application in the Earth's ionosphere (see for example Baumjohann and Treumann 1996). Note that the conductances at Earth are usually defined as integrals of the conductivities in the radial direction). We also note that (22.11) has the same structure as the more general equation for arbitrary magnetic field perturbations (Wolf-Gladrow *et al.* 1987, Neubauer 1998b).

An analytic solution. Equation (22.11) gives considerable insight into the local interaction at Io. We solve it for constant circular ionospheric conductances within a radius R and zero outside. Therefore we introduce cylindrical coordinates $x = r\cos\varphi$ and $y = r\sin\varphi$ and a perturbation electric field $\boldsymbol{E_p} = \boldsymbol{E} - \boldsymbol{E_0}$, and then write the interior solution, i.e., within Io's ionosphere for $r < R$ as

$$\Phi^i = \Phi_0 - E_p\,[\cos\Theta_p r\sin\varphi + \sin\Theta_p\, r\cos\varphi] \qquad (22.14)$$

and the exterior solution, i.e., for $r > R$

$$\Phi^e = \Phi_0 - E_p\left(\frac{R}{r}\right)^2 [\cos\Theta_p r\sin\varphi + \sin\Theta_p\, r\cos\varphi] \qquad (22.15)$$

The magnitude of the perturbation electric field is given by

$$E_p = E_0\sqrt{\frac{\Sigma_2^2 + \Sigma_1^2}{\Sigma_2^2 + (\Sigma_1 + 2\Sigma_A)^2}} \qquad (22.16)$$

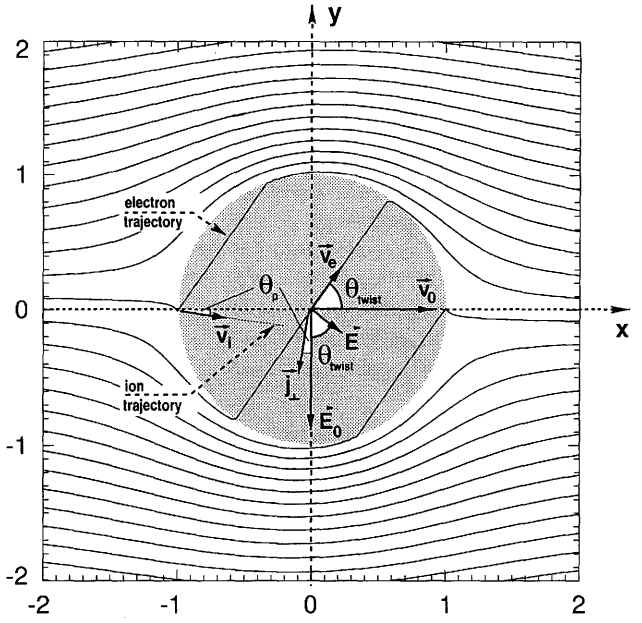

Figure 22.3. Behavior of basic properties close to Io from an analytic solution of the electric potential equation for constant Σ_1, and Σ_2 within a circle with radius R, and zero outside. Displayed are isocontours of the electric potential with $\Sigma_1 = 25$ S, $\Sigma_2 = 50$ S, $\Sigma_A = 5$ S, and the radius $R = 1$ of the ionosphere. Isolines are trajectories of the electrons. Inside $R = 1$, where Io is embedded, the flow of the electrons is rotated towards Jupiter and the ions slightly away from Jupiter.

and the angle Θ_p by

$$\tan\Theta_p = \frac{2\Sigma_A\Sigma_2}{\Sigma_2^2 + \Sigma_1(\Sigma_1 + 2\Sigma_A)} \qquad (22.17)$$

We display isolines of the derived solution in Figure 22.3.

Transforming to Cartesian coordinates, we obtain a constant electric field inside R given by

$$E^i = -\nabla\Phi^i = \boldsymbol{E_0} + E_p\begin{pmatrix}\sin\Theta_p\\ \cos\Theta_p\\ 0\end{pmatrix} \qquad (22.18)$$

The interior electric field for finite conductance is thus always reduced and rotated with respect to the undisturbed electric field $\boldsymbol{E_0}$. The rotation of the electric field can be significant and described by the angle

$$\tan\Theta_{twist} \equiv -\frac{E_x}{E_y} = \frac{\Sigma_2}{\Sigma_1 + 2\Sigma_A} \qquad (22.19)$$

(see Figure 22.3). Since isolines of the electric potential are trajectories of the electron flow, the general electron flow pattern can be seen in Figure 22.3, too.

This solution of (22.11) incorporates the main properties of Io's local interaction:

(i) The upstream plasma flow is strongly slowed in Io's ionosphere. The ionospheric plasma flow is reduced by $\alpha = E^i/E_0$ (see (22.18)) compared to the upstream flow. Neglecting the Hall conductivity, we find

$$\alpha = \frac{2\Sigma_A}{\Sigma_1 + 2\Sigma_A} \qquad (22.20)$$

(ii) Only a small fraction of the upstream plasma flow can enter Io's ionosphere. This fraction is given by the same α as in (i) (Southwood *et al.* 1980, Southwood and Dunlop 1984, Goertz 1980).

(iii) The rest of the upstream plasma is directed around Io's ionosphere. On the flanks of Io the flow is accelerated. The maximum speed for $\alpha = 0$ is twice the unperturbed velocity for the above solution.

(iv) The electron flow is strongly rotated in Io's ionosphere due to the Hall effect by Θ_{twist}. Thus more of the upstream plasma enters Io's ionosphere on the anti-Jupiter-facing side than on the sub-jovian side.

(v) The maximum ionospheric current is

$$J_{\text{total}} = 8\Sigma_A R E_0 \tag{22.21}$$

when the ionospheric conductances far exceed the Alfvén conductance, i.e., $\alpha = 0$. Then the maximum current flows and we describe the electric current system at Io as fully saturated.

(vi) On the basis of Equation (22.11), further quantities such as the electric current, the ion flow, etc. can be derived. (See for example Figure 22.3.)

22.2.4 The Far-Field Interaction

As argued in Section 2, the disturbance of the magnetospheric plasma of Jupiter by Io can be spatially divided into a near-field region (or local interaction) and a far-field disturbance region, where the former can be considered a sphere around Io's center with a radius of a few Io radii. The existence of the far-field region is obvious from observations and theoretical arguments.

The first observational evidence came from Io control of decametric (DAM) radio emissions. These emissions are well described by a model, in which the wave sources are distributed along the field lines connected to Io radiating very close to the local electron gyro frequency into hollow cones (see Section 22.4.2 below). The magnetic field (Acuña *et al.* 1981) and plasma disturbances (Belcher *et al.* 1981) observed during the *Voyager 1* encounter on 5 March 1979 around the closest approach distance of about 20 000 km are further evidence for a disturbance somehow connected to magnetic field lines passing through or closely by Io. Furthermore, the bright footprint in the jovian upper atmosphere (observed from the ground and HST) connected approximately to Io along field lines is the third piece of evidence (see Section 22.4.1 and Chapter 26). The body of this section deals with this type of disturbance which can be represented by a field of Alfvén waves initially radiated by Io, subject to some complications explained below.

From the theoretical point of view, we have the problem of sub-Alfvénic flow interacting with the body of Io and its volcanic atmosphere via a number of atomic or molecular processes. For simplicity we assume the plasma pressure p_t to be negligible compared with the kinetic pressure $p_k = \rho v^2$; $p_t \ll p_k \ll B^2/2\mu_0$, which is equivalent to $M_A \ll 1$ with the Alfvén Mach number M_A and the sonic Mach number $M_s \gg 1$ or the ratio $p_t/(B^2/2\mu_0) = \beta \ll 1$.

After the discovery of the Io effect by the Australian meteorologist Bigg (1964), initial modeling of the Io–Jupiter interaction was done under the impression that magnetospheric plasma densities must be very low, since (among other arguments) they did not affect decametric radio waves in their propagation to observers on Earth. The simplest description for the field disturbances connected with the magnetic field lines threading Io is the unipolar inductor model (Piddington and Drake 1968, Goldreich and Lynden-Bell 1969). In the unipolar inductor model, the plasma of the magnetosphere is described as a medium with infinite conductivity along and vanishing conductivity perpendicular to the magnetic field. In the early models the field-aligned currents generated by the motional electric field across Io close through the Pedersen conductance of the jovian ionosphere and Io's conducting interior. This assumption was later replaced by currents through Io's ionosphere involving Pedersen and Hall conductances. The total upgoing and downgoing currents I_{total} in each hemisphere are proportional to the conductance of the circuit composed of the jovian Pedersen resistance and the Pedersen resistance of Io connected in series. Since the currents in the magnetosphere flow along the distorted field lines, the direction of these currents varies with the magnitude of I_{total}. The distortion of the magnetospheric electric field near Io, i.e., mainly the reduction of the magnetospheric electric field E_0, increases with the ratio of Io's Pedersen conductance to the jovian Pedersen conductance. The distortion of the electric field implies distortions of the flow (see Figure 22.3), which then implies a general acceleration of the plasma. However, in the unipolar inductor model the currents in the magnetosphere are parallel to the field lines and thus exert no force on the plasma. This is possible only if the mass density is negligible. Hence the model can be valid only for relatively small densities and hence Alfvén Mach numbers M_A. In this model temporal variations in the conductances have immediate consequences in that the current system reacts without delay. The high propagation velocities of the responsible Alfvén waves then also require low densities. Magnetic fields and currents are shown in Figure 22.4 for the classical unipolar inductor model.

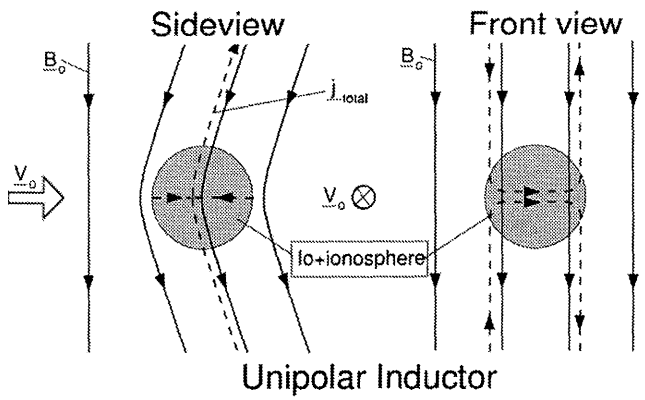

Figure 22.4. Side view and front view of the unipolar inductor model applied to Io. In the side view, one views towards Jupiter (behind Io), in the front view along the flow direction with Jupiter to the far left. Magnetic field lines are shown as solid lines and current stream lines dashed. At some distance from Io current vectors and magnetic field vectors are parallel or anti-parallel.

The discovery of the dense plasma torus at Io's orbital distance (approximately around the centrifugal equator of Jupiter as a whole) by the *Voyager* UVS experiment (Broadfoot *et al.* 1979) undermined the foundation of the classical unipolar inductor model except perhaps for Io at

maximum northern or southern magnetic latitudes, i.e., near torus edges. Inertial currents are not negligible any more and a full MHD description is necessary (Neubauer 1980). The significance of the mass density in the torus can be expressed by the Alfvén Mach numbers, which turned out to be $M_A \sim 0.15$ at the *Voyager 1* encounter and $M_A \sim 0.3$ at the *Galileo* encounters.

The MHD-disturbance field can most conveniently be described as a combination of MHD nonlinear wave modes, which interact with each other in the framework of the method of characteristics. The method of characteristics is a powerful tool for the description of linear and nonlinear disturbances in many fields of physics (Jeffrey and Taniuti 1964). Its fundamental idea is to introduce new coordinates along directions based on the propagation of weak disturbances, superimposed on disturbance fields of arbitrary amplitude to guide the solution. The new curvilinear coordinates are referred to as characteristics. Since Io moves with a velocity less than the fast magneto-sonic mode (see above) and is thus "sub-fast", no characteristics exist for the fast mode. Fast disturbances can escape in all directions. Thus the amplitude of fast mode disturbances must decrease as a function of distance from a source like Io and can be considered negligible in the far-field. Secondly, the slow magnetosonic mode does not exist because of our assumption $\beta = 0$, which will briefly be dropped at the end of this section. Thirdly, a degenerate convective disturbance mode exists with zero propagation velocity with respect to the plasma rest frame. It can convect away mass and pressure-balanced structures. Thus it describes Io's "mass loss tail." This mode is of interest as a source of the Io plasma torus, but outside the scope of this section. It has characteristics given by the streamlines of the flow.

The most important disturbance mode for the far-field is the Alfvén mode, which serendipitously also has characteristics even in 3D given by

$$C_A^+: \qquad \boldsymbol{v}_A^+ = \boldsymbol{v} + \frac{\boldsymbol{B}}{\sqrt{\mu_0 \rho}} \tag{22.22}$$

$$C_A^-: \qquad \boldsymbol{v}_A^- = \boldsymbol{v} - \frac{\boldsymbol{B}}{\sqrt{\mu_0 \rho}} \tag{22.23}$$

where $\boldsymbol{v}_A^+$ and $\boldsymbol{v}_A^-$ are referred to as Riemann invariants or sometimes Elsasser variables. They describe the causal relationship between the disturbance source, i.e., Io and its atmosphere, and the disturbance at any point, particularly in the far-field.

Let us assume for a moment that Io moves through a homogeneous plasma given by the local torus plasma parameters $\boldsymbol{v}_0$, $\boldsymbol{B}_0$, ρ_0 and yielding $\boldsymbol{v}_{A,0}^+$ and $\boldsymbol{v}_{A,0}^-$. Alfvénic disturbances, the most important disturbances in the far-field, can causally be connected to Io only along the characteristics pointing away from Io at the boundary between the far-field and the near-field defined above. These characteristics can be called "outgoing". Since the jovian magnetic field points from north to south, in the northern hemisphere of Jupiter Alfvén waves can come from Io only along $\boldsymbol{v}_{A,0}^-$ and analogously along $\boldsymbol{v}_{A,0}^+$ in the southern hemisphere. In the northern hemisphere $\boldsymbol{v}_A^-$ is constant everywhere and equal to $\boldsymbol{v}_{A,0}^-$ whereas $\boldsymbol{v}_A^+$ can vary as a function of location (Neubauer 1980) and vice versa for the southern hemisphere. The northern Alfvénic disturbances can be referred to as the northern Alfvén wing and analogously in the southern hemisphere, where the notation Alfvén wing was introduced in the linear theory used by Drell *et al.* (1965).

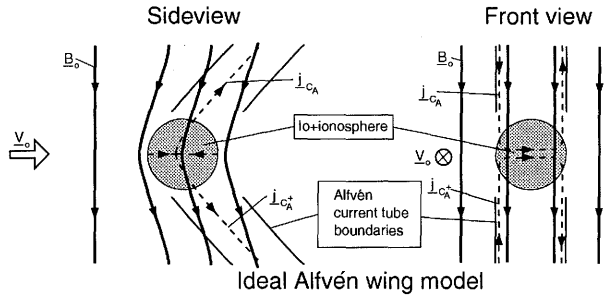

Figure 22.5. Side view and front views of the ideal Alfvén wing model applied to Io. In the side view one looks towards Jupiter (i.e., Jupiter is located behind Io). In the front view one looks along the flow direction with Jupiter to the far left. Magnetic field lines are shown as solid lines with arrows and current stream lines are dashed. The currents leaving the near-field region around Io or entering it are connected to currents along the Alfvén characteristics in the Alfvén current tubes of the far-field region. The boundaries of the current tubes are shown solid. In the far-field there also exist currents (not shown) perpendicular to the characteristics, which close on themselves.

Figure 22.5 illustrates the Alfvénic disturbances. Some magnetic field lines are shown by solid lines with arrows. The solid lines parallel to the characteristics $C_{A,0}^-$ in the northern hemisphere of Jupiter give the extent of a cylinder referred to as the current tube. It is only the region inside the current tube in which currents parallel to the characteristics $C_{A,0}^-$ or $\boldsymbol{v}_{A,0}^-$ are allowed. These currents illustrated by dashed lines on the far hemisphere of Io with respect to Jupiter can only be connected to the currents (mostly field aligned) injected from the near-field region of Io. However, there are also currents perpendicular to the characteristics, which close on themselves. The plasma and magnetic field disturbances extend beyond the current tube and taper off as a function of distance from the cylinder axis. Although superficially the situation looks similar to the unipolar inductor model there are important differences. The direction of the currents connecting to near-field currents is given by the direction of the characteristics $\boldsymbol{v}_{A,0}^{\pm}$ independent of the strength of the disturbance. The closure currents are generally not parallel to the magnetic field. The maximum current in the wings is determined by the Alfvén conductance and corresponds to J_{total} in Equation (22.21)

$$J_{\text{max, northern wing}} = J_{\text{max, southern wing}} = 1/2 J_{\text{total}} \tag{22.24}$$

The Alfvén wings would exist, even if no jovian ionosphere were present, as a fundamental solution.

We now drop the assumption that the plasma through which Io moves is a homogeneous plasma with physical parameters $\boldsymbol{v}_0$, $\boldsymbol{B}_0$, ρ_0 to consider the particular characteristics of Alfvén wave propagation through the Io torus, the high latitude magnetosphere and jovian ionosphere. Here the variation along a field line of the density and the Alfvén wave propagation velocity are important, i.e., $\boldsymbol{v}_A^+$ and $\boldsymbol{v}_A^-$. Both *Voyager* and *Galileo* observations have yielded the plasma properties quite well near the magnetic equator, but the densities are not known very well at higher latitudes, except that they are much smaller. Radio science observa-

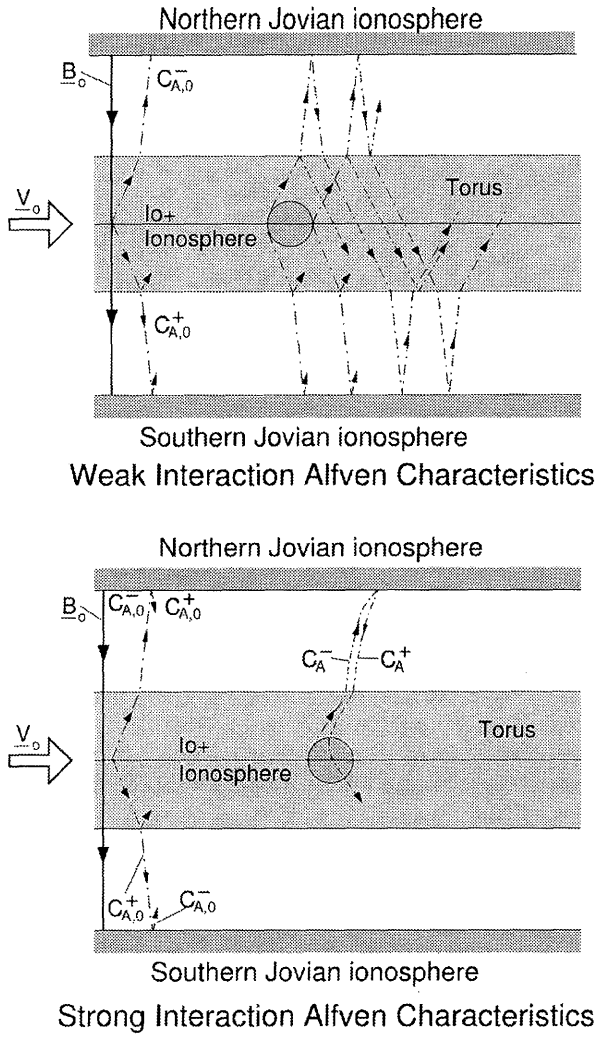

Figure 22.6. (a) Upper Figure: We show a schematic representation of the jovian magnetosphere with straight magnetic field lines (solid) through Io. The Alfvén characteristics (dot–dashed) issuing from the equatorial plane are defined on the left hand side. In addition, the characteristics going out from Io and its ionosphere are shown for Alfvén waves reflected and transmitted at the torus boundaries and ionospheric boundaries. Only these characteristics represent a causal connection to Io. For weak Alfvén waves the angle of incidence and the angle of reflection with respect to the boundary normals are equal. (b) Lower Figure: Same as Figure 22.6a except for the strong interaction of the nonlinear Alfvén waves. Here it has to be taken into account that the incident wave interacts nonlinearly with the reflected wave, which is illustrated schematically.

tions by the *Pioneer* and the *Voyager* missions have yielded electron densities in the jovian ionosphere. Thus the propagation speed of Alfvén waves along the field lines begins with several 100 $\mathrm{km\,s^{-1}}$ in the central region of the torus (Bagenal 1983), increases to close to the speed of light at the torus boundary with unknown details of the transition and decreases to a minimum of several 10^4 to 10^5 $\mathrm{km\,s^{-1}}$ at the ionospheric peak. Strong gradients in propagation velocity and density will lead to wave reflection, particularly at the torus boundary and/or the ionosphere.

Figure 22.6 illustrates this for two cases. In Figure 22.6a the case of a weak Alfvén wing is considered, where the perturbation of the magnetospheric electric field and the plasma velocity is small. This very unrealistic case, implying Alfvén conductance much greater than Io's Pedersen conductance, is just used for illustration. The characteristics of the reflected (incoming) waves are shown schematically. In this case the reflected waves pass a large distance downstream of Io. There is then no influence on the near-field perturbation of Io. The flow system near Io does not know about the existence of the reflecting torus boundary or jovian ionosphere. The interaction is strictly local. The condition for no feedback to occur is that the round-trip time of Alfvén wave propagation to a reflecting boundary $T_{\text{round-trip}}$ is greater than the time for a plasma parcel to cross Io's interaction region T_{passage} (Neubauer 1980, Southwood *et al.* 1980, Hill *et al.* 1983, Hill and Pontius 1998). The condition must be fulfilled for any Alfvén wave amplitude, i.e., for linear and also nonlinear waves. Here we have

$$T_{\text{round-trip}} = \int_{S_{C_A}} \frac{\mathrm{d}s}{v_{\text{Alfvén}(s)}} \tag{22.25}$$

$$T_{\text{passage}} = \int_{S} \frac{\mathrm{d}s}{v(s)} \tag{22.26}$$

S_{C_A} is the path along the Alfvén characteristic and S is a streamline through the interaction region leading to largest T_{passage}. $v_{\text{Alfvén}}$ is the propagation velocity of an Alfvén wave given by

$$\frac{1}{v^2_{\text{Alfvén}}} = \frac{1}{c^2} + \frac{\mu_0 \rho}{B^2} \tag{22.27}$$

with c the speed of light and $v(s)$ is the plasma velocity along a central stream-line of length L_c. In the case of a weak interaction we have $T_{\text{passage}} = L_c/v_0$ and for a strong interaction implying regions with $v(s) \ll v_0$, locally, $T_{\text{passage}} \gg L_c/v_0 = T_{\text{passage,min}}$. Assuming $L_c \sim 4$ R_{Io} and taking $v_0 = 57$ $\mathrm{km\,s^{-1}}$, $T_{\text{passage,min}}$ turns out to be 128 s.

Figure 22.6b illustrates the characteristics in the case of a strong Alfvén wing, which after reflection returns to Io. We note that the characteristics differ from the weak case. This is because in the weak case the characteristics are determined approximately by the properties of the unperturbed plasma, whereas in the strong disturbances case the characteristics are determined by the disturbed field and plasma parameters. For example, a reflected disturbance must move through the high latitude incident wave. The nonlinear reflection problem was first addressed by Goertz and Deift (1973). By increasing the interaction strength, feedback between the reflecting boundary, e.g., the jovian ionosphere, and Io can always be achieved. We obtain the following inequalities:

No feedback between Io and reflecting boundary:
$T_{\text{passage}} < T_{\text{round-trip}}$
$\Rightarrow$ Ideal Alfvén wing

Partial feedback between Io and reflecting boundary:
$T_{\text{passage}} \gtrsim T_{\text{round-trip}}$ (22.28)
$\Rightarrow$ Reflected wave reaches Io,
mixed Alfvén wave disturbance system

Strong feedback between Io and reflecting boundary:
$T_{\text{passage}} \gg T_{\text{round-trip}}$
$\Rightarrow$ Unipolar inductor

It is clear from the geometry of the characteristics of the reflected Alfvén waves returning to Io that there must always be a spatial region on the leading side (in the flow sense) of the total far-field disturbance system which can be described as a pure outgoing Alfvén wave. For this reason the magnetic field and plasma disturbances during the *Voyager 1* encounter could be well described as an outgoing nonlinear Alfvén wave. The spatial volume occupied by this ideal Alfvén wing portion decreases with decreasing ratio $T_{\text{round-trip}}/T_{\text{passage}}$. During a synodic rotation period of Jupiter as seen by Io, $T_{\text{round-trip}}$ varies from ~1000 s with Io in the center of the torus to much lower values like 450 s (Crary and Bagenal 1997) at maximum positive or negative magnetic latitude excursions. Realistic models of the near-field region (e.g., Saur *et al.* 2002) yield 4000 s for T_{passage}. Thus we generally expect the mixed Alfvén wave case between the ideal Alfvén wing and the unipolar inductor case. If the interaction strength does not vary, T_{passage} is about the same at the maximum magnetic latitudes and these cases are closer to the unipolar inductor. The situation is not much different for reflection at the jovian ionosphere and the torus boundary, since the difference in $T_{\text{round-trip}}$ should be small because of the low densities at high latitudes. Note, finally, that a remarkable coincidence exists for Io, since the Alfvén conductance in the torus happens to be not much different from the Pedersen conductances of Jupiter's ionosphere. This suggests that the influence of the details of the far-field disturbances on the plasma flow through Io's atmosphere is minor at least in the MHD picture.

No quantitative model of the mixed nonlinear Alfvén wave disturbance system launched by Io exists. There are some early ray tracing results (Bagenal 1983) and full linear wave solutions (Wright 1987). A substantial observational base exists in the phenomenology of the Io footprint observations covered in Section 22.4.1 for possible model validation. In addition to the spatial distribution of the Alfvén wave fields, the following issues need to be addressed: the question of the generation of the electron distribution functions to explain the radiation intensities measured in the footprints in Jupiter's high latitude ionosphere; the electron beams observed during some encounters of the *Galileo* spacecraft with Io (Williams *et al.* 1999); and the special electron distributions needed to explain the radio emissions via the magnetospheric cyclotron maser mechanism generally accepted and outlined in Section 22.4.2. The only work in this direction is the paper by Crary (1997), who considered Fermi acceleration of electrons by kinetic (non-MHD) Alfvén waves. Crary (1997) proposes strong multiple reflections of the nonlinear Alfvén wing at the torus boundary with strong feedback between Io and the torus boundary in our nomenclature. Relatively weak transmitted Alfvén waves are reflected many times between the jovian ionosphere region and the torus boundary in the same hemisphere, thus determining the geometry of arcs observed by the *Voyager* radio astronomy experiments. Observational evidence has been presented by Queinnec and Zarka (1998).

At the beginning of the discussions in this section we have assumed vanishing plasma pressure, i.e., $p_t = 0$, for simplicity. This corresponds to a sonic Mach number of $M_s = \infty$ for the incident flow. M_s based on observations

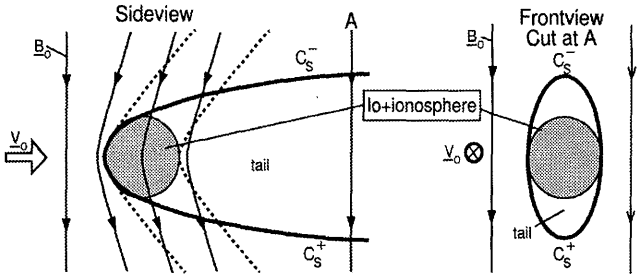

Figure 22.7. Same geometry as in Figure 22.5. The assumption of zero speed of sound has been dropped, but the sound speed is still much less than the Alfvén speed. The outermost slow MHD-characteristic connected to Io and its ionosphere is shown. The front view is combined with a cut through the tail of Io.

is closer to $M_s \geq 1$ and $M_f \ll 1$ in view of $M_A^2 \ll 1$. Dropping the assumption of $p_t = 0$ does not change the Alfvén wave fields very much. However, it leads to the occurrence of slow mode magneto-sonic waves (Neubauer 1980, Linker *et al.* 1988), which can be pictured as sound waves or even sonic shock waves essentially channeled along the magnetic field. Together with the non-propagating convective modes mentioned above and the feet of the Alfvén wings, they determine the real extent of the tail of Io in the direction along the magnetic field. Figure 22.7 illustrates the situation.

22.3 OBSERVATIONS OF LOCAL INTERACTIONS AND THEIR INTERPRETATION

We now turn to observations of Io's local interaction. In the first part of this subsection, we will mostly present the in situ observations obtained by the *Galileo* spacecraft. In the second part, we will focus on remote sensing observations of the local interaction. For the interpretation of the data, we consider the theoretical concepts introduced above and we refer, in particular, to several numerical models applied to Io's interaction.

22.3.1 *Galileo*: *In Situ* Measurements

Io's interaction was probed by the *Galileo* spacecraft with seven very close flybys. They are referred to as I0, I24, I25, I27, I31, I32, I33. The first *Galileo* flyby I0 in December 1995 probed the wake of Io at an altitude of ~900 km at closest approach. It yielded a wealth of unexpected and very surprising results. The I24 flyby can be considered as an upstream flyby with closest approach at a distance of 615 km. The I27 also started upstream, but then passed along Io's flanks through Io's ionosphere, with closest approach at a distance of only 200 km. For the I25 polar flyby a technical problem arose and only plasma wave data were acquired. The I31 and I32 flyby occurred in August and October 2001 and thus when this chapter was submitted results were not available in published form and we have referred to conference reports. During the I33 flyby no data were taken because the *Galileo* spacecraft went into a safe-mode. We now describe the results of these flybys depending on phenomena and location.

Plasma Density

Io's ionosphere and plasma environment is very strongly advection dominated and evolves with the plasma flow from the upstream to the downstream side. On the upstream side along the I24 trajectory, the electron density profile reported by Gurnett *et al.* (2001a) from Plasma Wave observations does not show any density enhancement above torus values and suggests that *Galileo* did not enter Io's ionosphere. It thus gives constraints on Io's upstream atmosphere. However, these measured densities are not in agreement with the measurements taken by the Plasma Science Instrument (Frank and Paterson 2000), which reported a factor of 3–4 enhancement with respect to the torus densities. In Io's ionosphere, *Galileo* measured strongly enhanced electron and plasma densities. The most pronounced density increase, by more than a factor of 10, was observed for the I27 flyby on the flanks (Gurnett *et al.* 2001a, Frank and Paterson 2001) with in situ PLS measurements. In the wake of Io the *Galileo* spacecraft measured about a factor five enhancement compared to the background densities (see Figure 22.8 and Gurnett *et al.* 1996, Frank *et al.* 1996).

Above Io's poles the electron density profile inferred from the plasma wave measurements shows a boxcar-like electron density distribution (Gurnett *et al.* 2001b). On field lines that roughly intersect Io's body, an electron density enhancement by about a factor of four was observed which dropped abruptly to torus values before and after entering this region. This density profile might be produced by the slow mode which transports plasma along the field lines. The plasma comes out of Io's dense low latitude ionosphere (Neubauer 2000) associated with the neutral density bulge around Io's equator observed by HST (Roesler *et al.* 1999, Strobel and Wolven 2001). Additional locally produced plasma in the polar atmosphere can be attributed to the polar volcanoes that have been observed recently. Linker *et al.* (2001) interpreted the density increase in terms of extensive pickup on slowed flow. The plasma science instrument observed, however, a decreased density by a factor of five for ions within an energy-to-charge ratio of 50 eV to 10 keV (Frank and Paterson 2002). This discrepancy may be explained by the slowdown of the flow to a bulk flow energy well below 50 eV and a thermal spread of velocities leading to reduced measured density.

The in situ measured plasma densities taken at equatorial latitudes of Io also agree qualitatively well with the *Galileo* spacecraft remote-sensing radio-occultation reported by Hinson *et al.* (1998). Average peak densities exceed 50 000 cm^{-3} and the ionospheric profile is remarkably similar to the ionospheric profile measurements reported nearly 25 years earlier by Kliore *et al.* (1975). The radio-occultation observations describe an ionosphere with a smaller density and scale height on the upstream side than on the downstream side, and maximum values at the flanks in agreement with a non-static, but strongly advection-dominated ionosphere.

Outside of Io's ionosphere in the Io plasma torus the plasma density varied from flyby to flyby between ~1000 cm^{-3} to ~3600 cm^{-3} (Gurnett *et al.* 1996, 2001a), Frank *et al.* (1996), Frank and Paterson (2000, 2001, 2002), compared with a maximum torus density of 2000 cm^{-3} observed by *Voyager 1*.

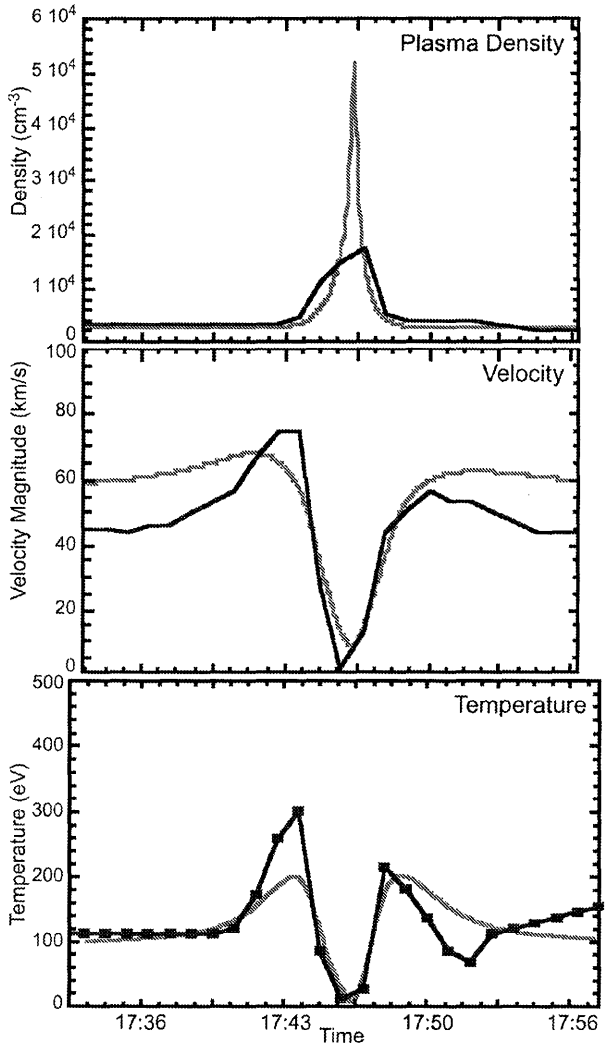

Figure 22.8. Plasma density, velocity and temperature for the first Io flyby in December 1995 (gray lines: numerical simulations by Linker *et al.* 1998; black lines: *Galileo* spacecraft observations).

Plasma Flow

The flow measurements, as reported in Frank *et al.* (1996), Frank and Paterson (2000, 2001, 2002), are in accordance with the picture of a plasma that is slowed in Io's ionosphere, redirected around Io and then re-accelerated in the wake (see Section 22.2.3 and Figure 22.3). The flow patterns are a non-local response to Io's electrodynamic interaction. This is particularly apparent outside of Io's ionosphere. For example, the flow is already significantly slowed upstream of the ionosphere. Deep in Io's ionosphere the flow is nearly stagnant with an observational upper limit of ~2 $km\,s^{-1}$ in the wake (I0) and at the flanks (I27) (Frank *et al.* 1996, Frank and Paterson 2001). Further away from Io on the flanks of Io's wake the plasma speeds up with a maximum plasma velocity of ~1.7 times the unperturbed flow (Frank *et al.* (1996) or see Figure 22.8 second panel). The plasma above the pole is also severely slowed, but shows a fast speed-up within several Io radii to the unperturbed velocities (Frank and Paterson 2002). *Galileo*'s radio-occultation measurements show independently that the downstream flow is re-accelerated to

unperturbed values already ~6 R_{Io} downstream of Io (Hinson *et al.* 1998). The reported polar slowdown of the plasma flow is consistent with the velocity profile within an Alfvén wing (e.g., Neubauer 1980 or Saur *et al.* 2002).

Much insight into the understanding and quantitative details of Io's plasma and field observations came from numerical simulation. The density, flow and temperature observations are in reasonable agreement with the numerical simulations for Io's local interaction by Linker *et al.* (1998) (see also Figure 22.8) as well as by Combi *et al.* (1998) and Saur *et al.* (1999, 2002).

Plasma Temperature

The unperturbed plasma temperature in Io's vicinity is ~10^6 K for all published flybys (Frank *et al.* 1996, Frank and Paterson 2000, 2001, 2002). Deep in Io's ionosphere and in the center of the ionospheric wake the measurements show a deep minimum of ~10^5 K, as evident in the I27 and I0 flybys. The I0 wake temperature minimum is surrounded by two maxima with temperatures up to 5 × 10^6 K. Using a simplified picture where we neglect multi-ion-fluid and kinetic effects, we can roughly learn from this temperature profile where the plasma originates or which part of the atmosphere it passed through. Freshly created pickup ions or ions that collide with neutrals acquire a temperature that corresponds to the local bulk flow velocity relative to the neutral atmosphere. The temperature minimum thus describes plasma coming from the downstream ionosphere, where the plasma speed is slow. The two temperature maxima describe plasma that comes from the flanks of the ionosphere, where the plasma is flowing fast. The most prominent signature of the temperature profile for the I30 polar flyby is a strong temperature increase by a factor of three on the downstream side (Frank and Paterson 2002). Currently, there are no measurements of the bulk electron temperature available.

The Magnetic Field

Io has a very interesting and complex magnetic field environment. Understanding its nature is a key to understanding Io's plasma interaction.

Upstream of Io's ionosphere along the I24 flyby, the magnetometer on board the *Galileo* spacecraft observed an increased magnetic field magnitude of 300 nT, due mostly to a perturbation component in the direction of the background field (Kivelson *et al.* 2001a). Along the flanks at the I27 flyby trajectory an increased magnitude was observed upstream of closest approach and a decreased magnitude downstream of it. The most surprising signature was however measured during the first Io flyby I0 through the downstream wake. The background magnetic field of 1850 nT decreased by as much as 700 nT due to a strong perturbation in the opposite direction to the background field (see Figure 22.9). This magnetic field perturbation was so strong that Kivelson *et al.* (1996a,b) and Khurana *et al.* (1997) concluded that Io must have an internal magnetic field directed opposite to that of the background field. This interpretation was questioned by others (Frank *et al.* 1996, Neubauer 1998a, Combi *et al.* 1998, Saur *et al.* 1999, 2002). This very controversially debated issue was in the end definitely resolved by the observations along the polar flybys I30 and I31 (Kivelson *et al.* 2001b). These measurements showed strong magnetic

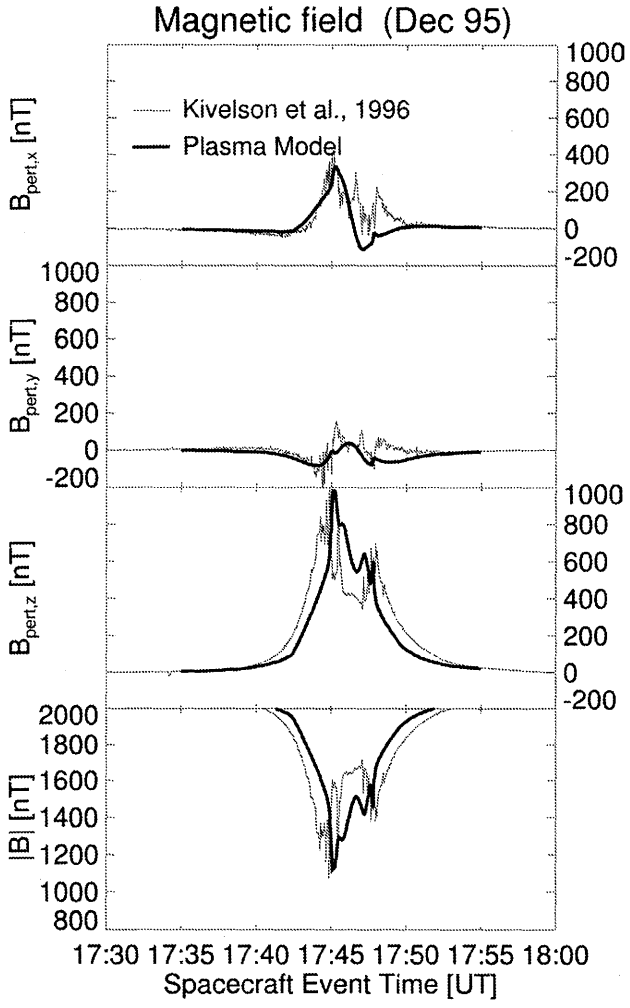

Figure 22.9. Magnetic field perturbation for the first downstream flyby I0 in December 1995. Observations by Kivelson *et al.* 1996 (thin solid line), and numerical model by Saur *et al.* 2002 (thick solid line).

field perturbations in the opposite direction to the unperturbed plasma velocity for I30 and along the flow for I31, as expected from an Alfvénic interaction, and ruled out an internal magnetic field.

Now we proceed to the physical interpretation of these observations together with some additional observational details.

Upstream: In the B,v framework, the interpretation of Io's magnetic field signature is particularly straightforward outside of Io's ionosphere where the frozen-in-field theorem holds. For the I24 trajectory *Galileo* passed upstream of Io's ionosphere. Elastic collisions and pickup in Io's ionosphere act as a force to slow the incoming plasma. This perturbation propagates upstream out of the ionosphere via the fast mode, and there the slowed plasma is responsible for an enhanced magnetic field magnitude, as can be seen very well in Figure 22.10, which shows a numerical simulation by Linker

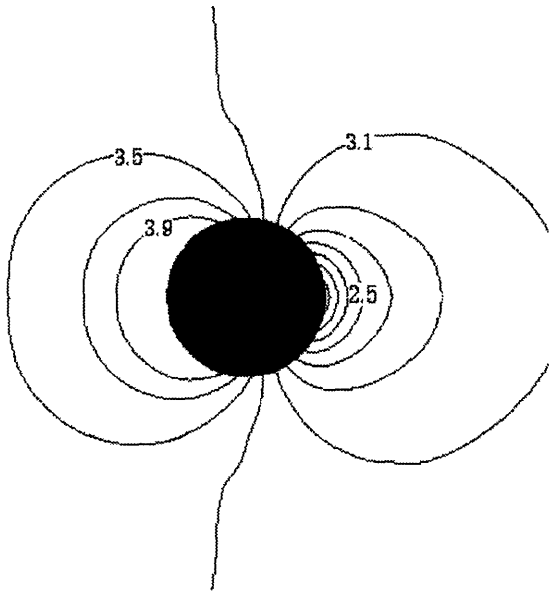

Figure 22.10. Self-consistently modeled magnetic field magnitude in a plane given by the background magnetic field and the velocity. A contour value of 3.2 corresponds to the background value of 1800 nT (from a slightly updated simulation of Linker *et al.* 1998).

et al. (1998). It displays the magnetic field magnitude in a plane given by the plasma velocity and the background field. In addition, the magnetic field lines are draped around Io (see Figure 22.5). This picture further explains that the resulting bending of the magnetic field lines creates on the northern hemisphere a component in the direction opposite to the incoming flow in agreement with the data of Kivelson *et al.* (2001a).

In the E,j picture, the magnetic field perturbation can be calculated directly from Biot-Savart's law (i.e., the integral form of Ampère's law) for a given current. For a pure qualitative estimate of the perturbation, one can simply use the right hand rule. Io's ionospheric current system carries a total electric current of about 10 million A through Io's ionosphere (Saur *et al.* 1999), which is divided partly into the upstream and partly into the downstream ionosphere (see Figure 22.2). On the upstream side the current produces a perturbation in the direction of the background field and thus an enhanced magnitude. This picture allows us to understand further details of the field: Since the I24 flyby was somewhat above Io's magnetic equator in the northern hemisphere, the upstream ionospheric current system produces a magnetic field perturbation component in the direction opposite to the unperturbed flow, and a component pointing away from Jupiter (see data shown in Kivelson *et al.* 2001a).

Downstream side: The magnetic field measurements for the I0 flyby through Io's wake (Kivelson *et al.* 1996a,b) is shown in Figure 22.9. Its general structure can be understood in the B,v picture with an argument analogous to I24 (see also Figure 22.10). A reduced magnetic field magnitude is expected on the downstream side of a conducting object where the slowed plasma flow is reaccelerated to upstream velocities due to the curvature of the bent-back magnetic field and the resultant Maxwell stresses (see Figure 22.5). In the E,j picture, the right hand rule gives on the downstream a signature in the opposite direction to the background field, and thus a reduction in the total magnitude.

The magnetic field measurements of the I0 flyby were simulated with different models. Linker *et al.* (1998) was able to reproduce the large scale structure of the I0 perturbation field both with and without the assumption of an internal magnetic field, while Combi *et al.* (1998) considered the non-internal magnetic field case to reproduce the observed large scale structure. Saur *et al.* (1999, 2002) applied a two-fluid model, which does not calculate the magnetic field self-consistently. But with their calculated anisotropic electric current system, their model can calculate the field perturbation with a Biot–Savart integral. It may be considered as the first order contribution in an expansion with respect to perturbation strength. It reproduces the overall perturbation and also details of the observations, such as the double peak structure caused by diamagnetic and inertial currents (see Figure 22.9).

From the increased magnitude of ~300 nT on the upstream side and a decreased component of ~600 nT on the downstream side, one can conclude that the total ionospheric electric current is not split equally on the upstream and downstream sides. There is more electric current closing in the downstream ionosphere, than on the upstream side. This is evidence for an atmosphere with a smaller scale height on the upstream side than on the downstream side, resulting from the drag force of the torus ions on Io's neutral atmosphere (Saur *et al.* 2002).

Along the flanks: The measured magnetic field profile along the I27 trajectory (Kivelson *et al.* 2001a) can be understood in several aspects as a mixture of the above discussed upstream and downstream cases. On the upstream side the magnitude is enhanced (as for I24) and on the downstream side it is diminished (as for I0). It is important to note that the frozen-in-field theorem applies only outside of Io's ionosphere. The I24 flyby occurred mostly in the northern magnetic hemisphere of Io, and thus the upstream and the downstream ionospheric equatorial currents produce a magnetic signature B_x in the opposite direction to the unperturbed flow. At locations just outside of the ionosphere, the ionospheric current system produces a magnetic field component B_y in the direction away from Jupiter, while within the ionosphere the components mostly cancel.

Above the poles: The reported magnetic field signature by Kivelson *et al.* (2001b) ruled out the possibility of an internal magnetic field on Io. An internal magnetic field would have yielded a strong component in the direction of the background magnetic field. The most prominent observed component is a strong signature in the direction opposite to the unperturbed flow in the northern hemisphere passes, as expected from an Alfvén wing bent back compared to the background field, and as simulated by Linker *et al.* (2001). It can also be explained with the electric current system along the Alfvén characteristics which are mostly in the downward direction on the Jupiter-facing side of the Alfvén tube and upward on the anti-Jupiter side. These measurements are in principle accordance with predictions by Saur *et al.* (2002).

Another interesting feature of the polar magnetic field observations, reported by Kivelson *et al.* (2001b), are im-

prints of Io's volcanic neutral atmosphere. Polar volcanoes create a locally enhanced neutral atmosphere, and consequently enhanced and inhomogeneous ionospheric conductivities. These local "conductivity hot spots" produce a local ionospheric electric current system. Current continuity requires current to flow in and out of the ionospheric hot spots mainly along the field lines and contribute a "small Alfvén wing" within the global wing. These small wings or "winglets" create magnetic field signatures which have been seen by the *Galileo* magnetic field measurements as presented by Kivelson *et al.* (2001b) and which have been independently simulated by Strobel *et al.* (2001). These effects of Io's patchy atmosphere on its interaction have also been anticipated and discussed in Neubauer (1998b, 1999). This opens the magnetometer as a new device with which to monitor Io's atmosphere.

Io's polar magnetic field signature give insight into both Io's Alfvén wing system and Io's ionospheric current system. Regions with a dense neutral atmosphere also create large Hall conductances which rotate Io's electric field. This rotated electric field is mapped out along the field lines and creates rotated Alfvén wings as could be seen in I32, in agreement with predictions by Saur *et al.* (2000, 2002).

Mass Loading and Elastic Collisions

As discussed in Section 22.2, the main reason for Io's electrodynamic interaction is the deceleration of plasma flowing past Io due to elastic collisions with the neutral atmosphere and due to mass loading. Saur *et al.* (2003) show that the effect of elastic collisions is greater than that of mass loading by a factor of 100 for realistic atmosphere densities. Thus, elastic collisions (in which we include charge exchange) are mostly relevant for the large scale features of Io's electrodynamic interaction, such as the slowing of the flow, its strong magnetic field perturbation and the creation of its Alfvén wings. The two main plasma sources (hence causes of mass loading) are electron impact ionization and photoionization. For a pure SO_2 atmosphere, Saur *et al.* (1999, 2003) showed that the total ionization rate due to photoionization is smaller than the electron impact rate. While less significant electrodynamically, mass loading has other important effects, however, such as the creation of Io's ionosphere, small scale magnetic field perturbations discussed below and importantly the mass loss tail of Io.

Plasma Waves

During the inbound pass through the Io plasma torus, the *Galileo* wave instrument observed a broad variety of plasma waves, such as jovian radio emissions, narrow-band, upper hybrid band and whistler-mode emissions (Gurnett *et al.* 1996). The upper hybrid frequency can be used to determine the electron density discussed above. As discussed for the I0 wake flyby, the whistler noise became particularly intense around closest approach to Io when high energy bi-directional electron beams were observed (see discussion of the observations by Williams *et al.* (1996) below).

Energetic Particle Measurements

During the wake flyby (I0), energetic particles were observed by Williams *et al.* (1996, 1999). The energetic electron pitch angle distribution evolved from a pancake distribution to a butterfly distribution function as *Galileo* approached Io. Near closest approach, in the wake of Io, the distribution suddenly turned into an intense bi-directional beam aligned with the magnetic field, and orginating close to Jupiter (Williams *et al.* 1999). Its spectra follow a power law in the energy range 15 keV to ~200 keV and correspond in this energy range to an energy flux of 3×10^{-6} J m^{-2} s^{-1} in each direction. No ion beams were observed on this flyby. While the electron butterfly distribution can be explained as an adiabatic response of the jovian energetic electron distribution to the changing magnetic field (Thorne *et al.* 1999), the mechanism for the electron beam is not understood (see proposed explanation by Chust *et al.* (2001)). As Mauk *et al.* (2001) point out, these electron beams are probably not responsible for the creation of Io's footprints in Jupiter's atmosphere.

The energetic particle detector, observed no electron beams along the I24 and I27 trajectory (Mauk *et al.* 2001). During the I27 flyby there might be some slight contribution around closest approach (D. Williams, private communication). Along the polar flybys I31 and I32 on field lines connecting to Io, mono-directional instead of bi-directional electron beams were observed. The component of the distribution with velocities coming from Io is cut out by Io, which is further evidence that the electrons are not accelerated close to Io (D. Williams, private communication).

Summary

The observations acquired during the I0 flyby in December 1995 witnessed an interaction that was stronger than expected from *Voyager*-era observations. Torus plasma densities were about a factor of two higher, an intense magnetic field perturbation was observed (most likely a consequence of an enhanced total electric current), the plasma flow was very strongly reduced and intense bi-directional electrons were present in the wake. A possible cause for the changes observed might be the variability of Io's volcanic activity that modified the neutral atmosphere and resulted in stronger plasma interactions in a denser torus.

22.3.2 Small-Scale Magnetic Field Perturbations

In the above Section 22.3.1 we mainly discussed large scale features of Io's plasma interaction. The high temporal resolution of the magnetic field data allows one also to study very interesting small-scale features related to microscopic processes.

Along the I0 trajectory the magnetic field data show very clear signatures of ion cyclotron waves on the inbound pass starting at a radial distance of ~15 R_{Io} (Kivelson *et al.* 1996b). The observed small-scale perturbations then turn into mirror mode waves close to Io, i.e., on plasma streamlines that have passed through the flanks of Io's ionosphere, and further away, on the outbound pass, ion cyclotron waves are observed again. The fluctuations reach a maximum of

250 nT and their power falls off with a power law with exponent of −3 with distance on the inbound pass and with a power law of −3.5 on the outbound pass. Kivelson *et al.* (2001a) also show that the wave power of the ion cyclotron waves peaks at the gyro-frequency of SO_2^+ or ions with equivalent mass to charge ratio.

Further theoretical analysis on these fluctuations came from work by Huddleston *et al.* (1997), Warnecke *et al.* (1997), and Huddleston *et al.* (1998). New ions generated in the vicinity of Io create ring-type ion distributions which are highly unstable and generate the observed ion cyclotron waves. Calculations using the warm dispersion relation indicate that the growth rate of SO_2^+ dominates the rates of S^+ and O^+, mainly due to the absence of a thermalized background component of SO_2^+, which would otherwise damp the waves. This damping occurs strongly for O^+ and S^+ because of the large thermalized torus O^+ and S^+ background densities. Huddleston *et al.* (1997) inferred from the magnetic field measurements a total ion production rate of $\sim 8 \times 10^{26}$ s^{-1} locally near Io.

In an analysis of the I24 flyby Russell and Kivelson (2000) find a clear signature of SO^+ ion production. The overall picture gathered from the I0 and I24 flyby was that the exosphere appears to be both spatially and temporally variable, possibly due to a time variability of the neutral source. Kivelson *et al.* (2001a) also discuss this asymmetry and show that for both I24 and I27 ion cyclotron waves are present on the downstream hemisphere, but are unimportant on the upstream side (i.e., $x < 0$).

22.3.3 Io's Aurora

Remote sensing observations by HST (Roesler *et al.* 1999, Retherford *et al.* 2000), by the *Galileo* spacecraft (Geissler *et al.* 1999, 2001), or by ground-based observations (Oliversen *et al.* 2001) of Io's atmospheric emissions are not only a powerful tool for monitoring Io's neutral atmosphere as discussed in Chapter 19, but they also provide information very valuable for the study of Io's electrodynamic interaction. In Figure 22.11a we show Io's ultraviolet aurora observed by HST. Remarkably, the brightest spots are in Io's magnetic equator and not at Io's pole. The brightest spots in addition do not remain at a fixed position in an Io-centered coordinate system, but rock up and down so that they stay in Io's magnetic equator given by Jupiter's changing background magnetic field at the location of Io. The radiation is produced by impact excitation of neutral atoms by hot electrons. In Saur *et al.* (1998) and Saur (2000) an explanation for the radiation morphology is presented. The main idea is that Io's electrodynamic interaction causes an inhomogeneous flow of upstream electron energy into Io's atmosphere. Due to the interaction, only a small fraction of the hot torus electron flux tubes can enter Io's ionosphere (see Eq. (22.20)), while the electron flux tubes can reach Io's flanks very easily. Consequently, more radiation is observed at these points. At the same time, electron energy is transported into Io's ionosphere along the flux tubes from the torus "above" or "below" Io (i.e., electron heat conduction in the fluid picture). This causes the spots to rock with the field line tangents above and below Io's equator. The anti-Jupiter side is brighter in this set of observations due possibly to the Hall effect, which rotates the electron

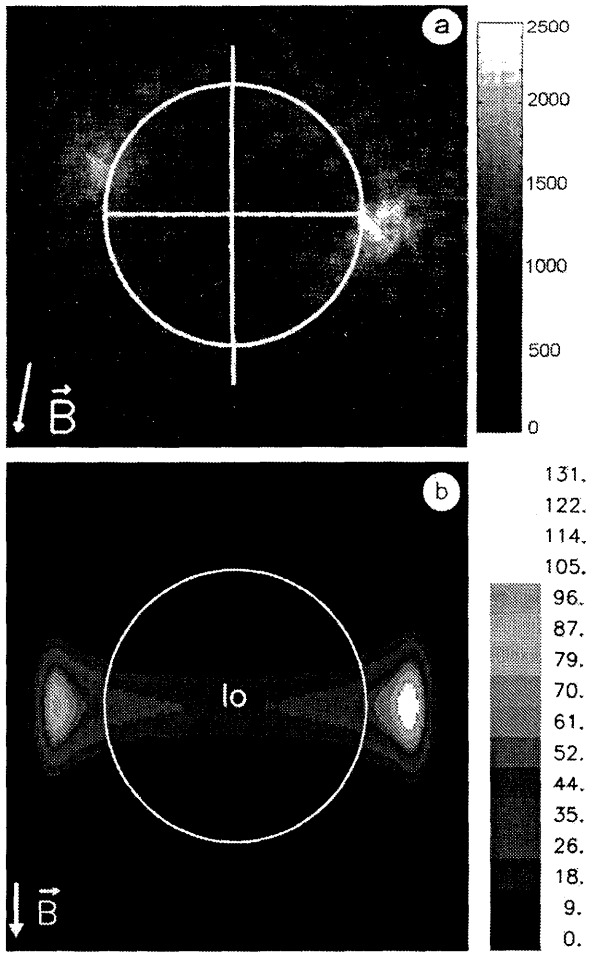

Figure 22.11. Io's aurora. (a) Reprint of Io's observed aurora for OI 135.6 nm (Roessler *et al.* 1999). Basic features are two equatorial maxima lying along a plane perpendicular to the local jovian magnetic field about 200 km above Io's limb, one in the sub-jovian hemisphere and the other in the anti-jovian hemisphere. The anti-jovian spot is brighter. (b) Io's simulated aurora (Saur *et al.* 2000).

flow in Io's vicinity so that the electrons enter Io's atmosphere preferentially on the anti-Jupiter side. Linker and McGrath (1998) also simulated Io's UV patterns. They used a one-fluid MHD model to calculate Io's radiation from the plasma temperature. However, the radiation is controlled by the electron temperature, which is decoupled from the ion (and in this case the plasma) temperature on Io's timescales.

Io's visible aurora as shown by Geissler *et al.* (2001) also reveals near-equatorial spots that rock slightly up and down, but less strongly than for the UV radiation. Because of the lower energy necessary to excite visible radiation, the morphology of the radiation depends much less on the electron temperature differences controlled by the local magnetic field, and thus more on the neutral atmosphere.

22.4 FAR-FIELD EFFECTS AND THEIR IMPLICATIONS

Far-field effects of the Io–Jupiter interaction include acceleration and precipitation of electrons into Jupiter's ionosphere

leading to UV, IR and radio emissions at/near the Io Flux Tube (IFT) footprints (cf. the review by Bhardwaj *et al.* 2001, as well as Chapter 26 on Jupiter's aurora). Remote observations are well adapted to study these electromagnetic signatures, whose existence demonstrate that Io's influence extends down to Jupiter's ionosphere. They are complementary to in situ observations close to Io. Besides these observations (IFT footprints and observations close to Io), nothing is known about the disturbance induced by Io except for some indirect information from radio emission (see below). *Galileo* and HST observations have shown similar but less energetic effects to occur at the footprints of the other Galilean satellites (see, for example, Hospodarsky *et al.* (2001) and Chapters 21 and 26).

Important information that can be derived from footprint electromagnetic emissions is their "lead angle". The perturbation of the jovian field by Io, which ultimately causes electron acceleration, needs some time to propagate from Io to the planet. Because the plasma is roughly corotating, one expects a longitude shift between the field line where the radio, UV or IR emission is produced (in or above Jupiter's ionosphere) and the instantaneous Io field line. This shift of longitude is referred to as "lead" angle because the emissions are produced ahead of Io in the direction of its orbital motion, i.e., towards smaller SIII longitudes. Accurate measurements of the variations of this lead angle versus Jupiter's rotation and Io's magnetic latitude should help to identify the type of the intervening Io–Jupiter interaction: unipolar inductor (corresponding to a relatively large lead angle, $\geq 12°$ (Goldreich and Lynden-Bell 1969), depending on the conductivities in Jupiter's and Io's ionosphere, but not on the density in the Io plasma torus), or Alfvén wings (corresponding to a smaller angle, $\leq 12°$, strongly varying with Io's magnetic latitude), as discussed in section 22.2.4.

Other measurements of interest include multiple spots, as well as a faint extended trail in the ionosphere downstream of Io's footprint, as observed in infrared H_3^+ emissions by Connerney and Satoh (2000) and in UV by Clarke *et al.* (2002). The former could result from multiple Alfvén wave reflections between the torus and the ionosphere (Figure 22.6). The latter was suggested to arise from wave reflection and attenuation (Delamere *et al.* 2003), wake reacceleration (Hill and Vasyliūnas 2002), or slow mode waves or shock waves excited by Io's motion through the plasma torus (Erkaev *et al.* 2002, Zarka *et al.* 2002).

22.4.1 Footprint Emissions at IR and UV Wavelengths

The detection of infrared emission at the foot of the Io Flux Tube (IFT) (Connerney *et al.* 1993) provided a new and powerful diagnostic for the Io interaction. Connerney *et al.* (1993) used NASA's 3 meter telescope atop Mauna Kea, HI, to image H_3^+ emission on Jupiter, using the Infrared Telescope Facility's (IRTF) new infrared array camera (ProtoCAM and subsequently NSFCAM) and a narrow-band filter centered at 3.4 microns. H_3^+ is the dominant ionospheric ion between about 1 and 100 microbars pressure level in Jupiter's atmosphere. It has many strong emission lines in the 3–4 micron window, and is particularly easy to directly image at 3.4 microns wavelength where a deep methane absorption band removes all light from below the homopause. In images of H_3^+ on Jupiter, one can identify intense and omnipresent auroral emissions (Connerney *et al.* 1993, Satoh *et al.* 1996, Satoh and Connerney 1999) at high magnetic latitudes, as well as a bright and isolated emission feature that marks the passage of the IFT footprint in Jupiter's ionosphere. The IFT footprint was subsequently identified in ultraviolet (UV) images (Clarke *et al.* 1996, Prangé *et al.* 1996) obtained with HST and with the visual imager on *Galileo* (Vasavada *et al.* 1999). The fainter flux tube footprints of Europa and Ganymede have been identified in the UV as well (see Chapters 21 and 26).

Measurements of the southern IFT footprint observed in the IR yielded a lead of 15 to 20 degrees (Connerney *et al.* 1993). Subsequent observations in the UV obtained with the HST led to estimates of 0 to 15 degrees of lead (Clarke *et al.* 1996, Prangé *et al.* 1996) and implied measurable time variations in the lead angle.

All such estimates necessarily depend heavily on the accuracy of the magnetic field model used to calculate the undisturbed position of the IFT footprint linked to Io's position. The early estimates used the GSFC "O6" magnetic field model (Connerney *et al.* 1993) for this purpose. The accuracy with which the position of the IFT footprint could be determined with this model was estimated to be no better than about ± 10 degrees in longitude (Connerney 1992), so the lead of the IFT could not be determined with great confidence. This implies that the measured UV and IR leads are not mutually inconsistent. As an increasing number of IFT footprint observations became available, they were used as a constraint to improve models of the jovian magnetic field (Connerney *et al.* 1998) and as of this writing it is clear that additional improvements are needed before the lead of the IFT footprint, and its dependence on System III longitude (λ), time, and local time, will be well understood.

The intensity of emission at the foot of the IFT is also known to vary with time, both in the IR and in the UV. The intensity of emission at the foot of the IFT is measured with some difficulty in the IR due to limited spatial resolution (about 1/2 arcsec) proximity to the bright auroral emissions, and variations in atmospheric seeing. These difficulties are mitigated in HST observing, but the limited availability of HST time and a significant sampling bias makes it difficult to separate time variations and System III variations. There is good evidence in the infrared observations of H_3^+ for a persistent and systematic variation of intensity of the IFT footprint with System III longitude (see Chapter 26). At northern latitudes, the footprint is 5 to 10 times brighter in regions $360° > \lambda > 275°$ where the northern field magnitude is weak, than it is in the region $200° > \lambda > 90°$ where the northern field magnitude is large. The southern IFT footprint is much brighter at longitudes where the northern foot is dim, and vice versa. This behavior suggests that the strength of the Io interaction is modulated by the surface magnetic field strength, as originally suggested by Dessler and Chamberlain (1979) and Dessler and Hill (1979). It is also consistent with the longitudinal variations of radio emission brightness as described in Section 22.4.2.

22.4.2 Radio Emission

The Io–Jupiter interaction was first revealed by the discovery that the occurrence of part of Jupiter's decameter emis-

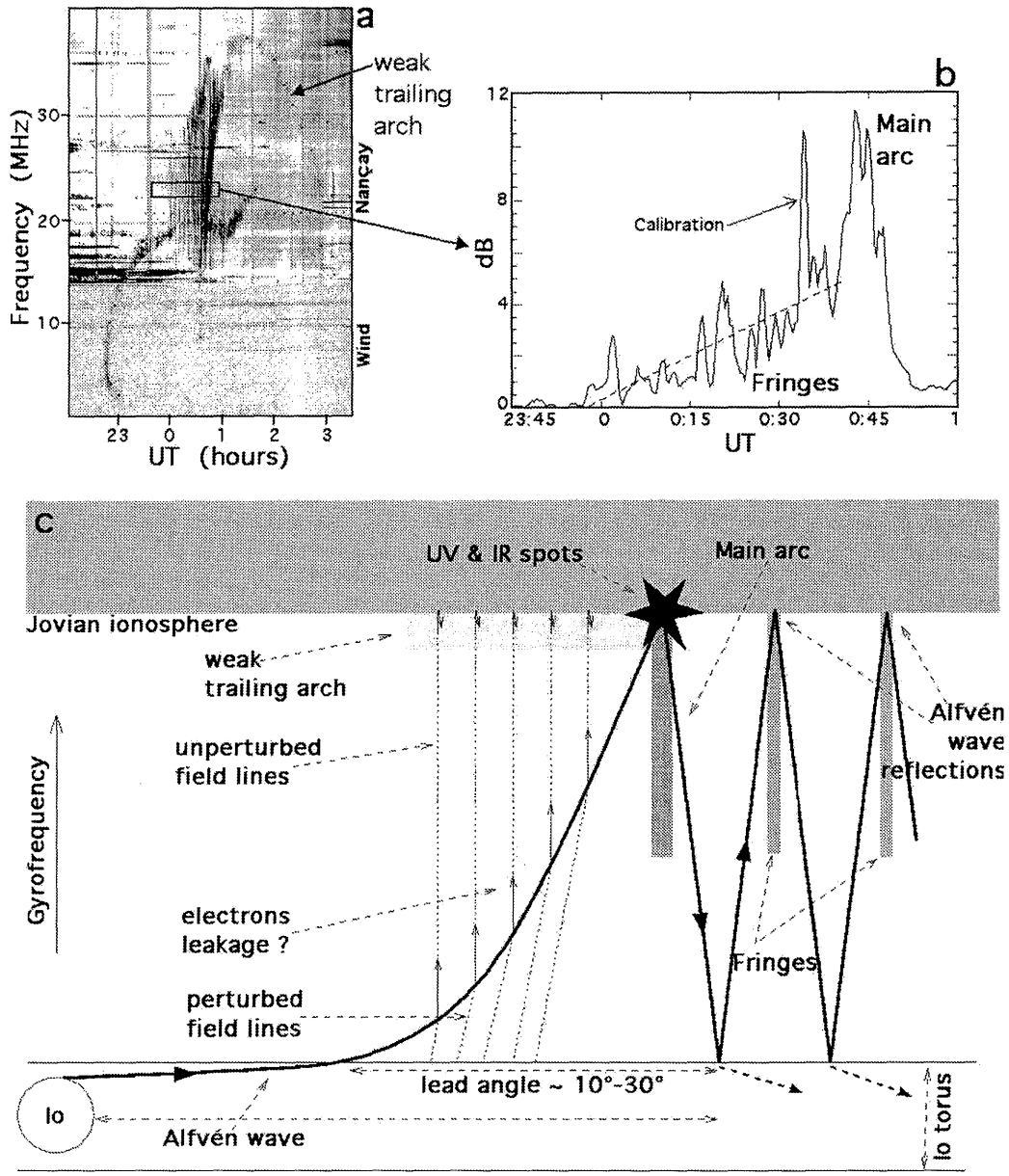

Figure 22.12. (a) Dynamic spectrum of typical Io-DAM arcs, detected over their whole frequency range combining *Wind* and Nançay data. The gray-scale intensity covers 3 dB above the background. Horizontal lines are man-made interference, vertical lines (in Nançay data) are calibrations or terrestrial lightning. (b) Intensity profile integrated over a 1 MHz band at 23 MHz, showing the main arc preceded by fringes with ~2 min spacing and ~ ×1.05 intensity ratio from one fringe to the next (dashed line). Intensity in the main arc is ~5 dB stronger than the first fringe before it. (c) Scenario for the Io–Jupiter interaction deduced from (a) and (b). The Alfvén propagation time (and hence lead angle) is accumulated mainly in the torus. Close to Jupiter, parallel electric fields in the Alfvén wing accelerate electrons, which decouple from it and precipitate into the ionosphere. Their reflected distribution possesses a loss-cone able to destabilize radio waves in a limited frequency range above the reflection level (light shading). Most of the energy is deposited at the first arrival of the perturbation to the ionosphere (star), causing particle acceleration and thus broadband radio emission (dark shading). Subsequent multiple reflections of the Alfvén wave between the ionosphere and torus produce the fringes observed prior to the main arc due to their larger lead (for a given radio beaming angle, the lead angle of the observed flux tube decreases with time).

sion (Io-DAM) was correlated with or "controlled by" Io's orbital position relative to the observer (Bigg 1964). This was the first clue that Io's motion in the jovian magnetosphere induces electron energization and precipitation. The decameter component independent of Io (non-Io-DAM), extending to lower frequencies down to fractions of a MHz, is of auroral origin and is thus the jovian counterpart of other planets' auroral radio emissions, like the Auroral Kilometric Radiation of the Earth (Zarka *et al.* 2001). Those emissions are produced by energetic electron precipitation in the auroral regions magnetically connected to distant parts of the magnetosphere (>20 R_J in the case of Jupiter).

Io-DAM and non-Io-DAM have many properties in common (cf. Zarka (1998) and references therein): both are produced along field lines at high magnetic latitude (with footprints at ~65° north and south for Io-DAM, and probably

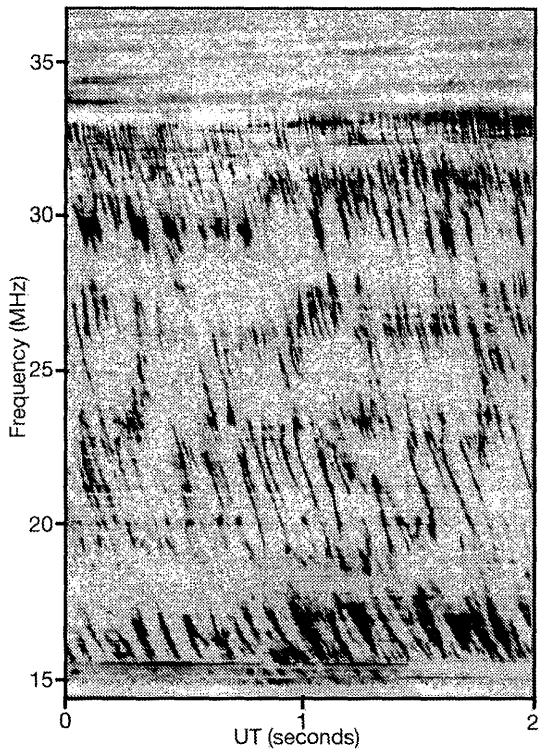

Figure 22.13. High resolution dynamic spectrum of jovian S-bursts recorded in Nançay (on April 7, 1995, 04:41) with an acousto-optical spectrograph. Frequency drifts versus time are mostly negative.

$\sim$75° – the latitude of the main auroral oval – for non-Io-DAM), close to the local electron cyclotron frequency, in the extraordinary (X) magneto-ionic mode, with elliptical polarization; both radio emissions are beamed at a large angle from the magnetic field at the source; their high-frequency cut-offs correspond to the highest gyro frequencies at the relevant magnetic field line footprints, i.e., $\sim$40 MHz in the northern ionosphere and 30–35 MHz in the southern one.

Differences between Io-DAM and non-Io-DAM include (1) occurrence rate, (2) low-frequency limit, (3) frequency-time (f–t) structure, and (4) solar wind control:

(1) Io-DAM occurrence is limited to two specific ranges of Io's orbital phase (Io $\sim$90° and $\sim$230°, as measured counterclockwise from the anti-observer direction), corresponding to Io close to maximum elongations to the east and west of Jupiter (in the reference of an observer on Earth, say, looking up at Jupiter in the sky);

(2) Io's control on DAM emission disappears below 1–2 MHz;

(3a) on timescales of minutes to hours, Io-DAM is structured in "arcs" in the f–t plane (Figure 22.12a) (Carr *et al.* 1983);

(3b) on timescales of milliseconds, Io-DAM often consists of intense sporadic bursts (called S-bursts, where "S" stands for "Short") drifting in the f–t plane at tens of MHz s^{-1} (Figure 22.13);

(4) Io-DAM activity is independent of solar wind fluctuations while non-Io-DAM is correlated to them (Genova *et al.* 1987).

The similarities suggest that Io-DAM and non-Io-DAM are produced by the same microscopic generation mechanism, most likely the cyclotron-maser instability, which feeds upon unstable electron populations with 1–10 keV characteristic energy (see LeQuéau (1988), Zarka (1998), and Chapter 26). The differences are attributed to different conditions under which the mechanism operates, e.g., the spatial and temporal structure of electron precipitations, and magnetic field line topology.

Below, we discuss the present knowledge of topics (1) to (4) and briefly address the energetics of footprint electromagnetic emissions.

Specific Characteristics of Io-DAM

(1) To first order, symmetrizing the east and west geometries of detection of Io-DAM implies a lead angle about 20° and a radio beaming angle relative to the local magnetic field about 70° (Goldreich and Lynden-Bell 1969, Zarka *et al.* 1996). However, a larger lead is required to make the instantaneous maximum frequency of Io-DAM compatible with model surface gyro frequencies in the hemisphere facing the observer. Up to 70° of lead was required with the early octupole "O4" model of the jovian field (Genova and Aubier 1985). This number was reduced to less than 40° in the frame of the more recent "O6" and "VIP4" models (Connerney 1993, Connerney *et al.* 1998, Queinnec and Zarka 1998), but it remains significantly larger than the measured lead of IR and UV spots ($\leq$20° – see above) even taking into account the $\sim$10° uncertainty in computed magnetic footprints. It was recently found (Zarka *et al.* 2002) that intense radio arcs all have a lead $\leq$15–20°, while only weak emissions as the trailing arch of Figure 22.12a have a larger lead. The latter could thus be the radio counterpart of the faint extended IR and UV trails detected downstream of Io's footprints, and could be interpreted, as mentioned above, in terms of wave reflections (Delamere *et al.* 2003), wake reacceleration (Hill and Vasyliūnas 2002), or of slow mode waves or shocks excited by Io (Erkaev *et al.* 2002).

Studying Io-DAM arcs from the northern hemisphere, Queinnec and Zarka (1998) found radio fringes with $\sim$2 minute spacing preceding the main arc (Figure 22.12a,b), and explained them by multiple reflections of the Alfvén wave perturbation between Jupiter's ionosphere and the external boundary of the torus (as proposed by Gurnett and Goertz (1981) and Bagenal and Leblanc (1988)), for which they could estimate a reflection coefficient of $\sim$ 95%. Their counterpart in UV and IR should be series of spots separated by 1° to 2°, as reported above. Connerney and Satoh (2000) have observed multiple features at the foot of the Io flux tube in H_3^+ imagery with approximately 4 to 5 degrees separation between subsequent spots. Multiple features are infrequently observed but on several occasions a pair of emission features has been observed in both H_3^+ imagery (Connerney and Satoh 2000) and in the UV (Clarke *et al.* 2002). Queinnec and Zarka (1998) also proposed an alternative scenario for the weak radio arc following the main arc (Figure 22.12a,c), in which accelerated electrons "leak" from the Alfvénic perturbation on their way to Jupiter, and produce – after mirroring – low intensity radio emission in a narrow band just below the maximum surface gyrofrequency.

(2) Combining ground-based and spacecraft observations, Io-DAM arcs can be observed from $\sim$40 MHz down to $\sim$1–2 MHz (Figure 22.12a), i.e., from just above the

ionosphere to 1–2 R_J above it. Their low-frequency cut-off lies between 1 and 2 MHz, in spite of the fact that the minimum electron gyrofrequency along the Io field line is ~60 kHz. Zarka *et al.* (2001b) have proposed that Io-DAM is produced along field lines threading through the dense, stagnating plasma wake discovered by *Galileo* (Gurnett *et al.* 1996); the vertical extent of the wake can then lead to quenching of the cyclotron-maser mechanism below 1–2 MHz, provided that it contains protons with a concentration >1–3%. Another consequence is that the longitudinal extent of Io's wake should be at least equal to the lead of "main" Io-DAM arcs, i.e., 15–20°.

(3a) Explanation of the radio arc shapes is a longstanding problem (Goldstein and Goertz 1983). Queinnec and Zarka (1998) performed 3-D modeling over the full 1–40 MHz frequency range (Figure 22.12a), using the O6 and VIP4 field models, and showed that the arc shape is quantitatively consistent with the emission coming from a single flux tube fixed in Io's frame, leading Io by ~10°–30°. The detailed arc shape results from the combination of non-planar field line topology with radio emission beaming in a conical sheet of $70 \pm 5°$ aperture (half-angle) and $\leq 2°$ thickness (Kaiser *et al.* 2000). The radio beaming angle must slightly decrease with increasing frequency (Lecacheux *et al.* (1998) showed that the arc shape cannot be matched with a constant beaming angle).

(3b) S-bursts are detected only a few percent of the time, in very specific configurations of Io, Jupiter, and the observer. This can be attributed to a small source size and a very narrow beaming of the emission. Flux densities may reach 50 times that of slowly varying emission, but the average power of the bursts is only $\sim 10^{8-9}$ W (versus $\sim 10^{10}$ W for the slowly varying emissions) (Queinnec and Zarka 2001). S-bursts are instantaneously narrow-banded (a few kHz) and very sporadic (fixed-frequency duration of a few milliseconds) (Ellis 1982). Their *f*–*t* structure consists mainly of a fast negative drift from high to low frequencies, at typically -10 to -30 MHz s^{-1} (Figure 22.13). On the average, the drift is consistent with the adiabatic motion of electrons with ~5 keV energy (and pitch angle ~2–3° at equator), moving upwards from their mirror point at $\sim 2 \times 10^4$ km s^{-1} (Zarka *et al.* 1996). But individual bursts have a much more complex morphology. (Note that if the *f*–*t* drift is indeed due to electron motion, its abrupt variations could be the signature of magnetic-field-aligned potential drops in the IFT.) Very high resolution observations revealed a burst sub-structure consisting of many short (<1 msec) narrow-band (<1 kHz) >10 dB spikes, sometimes even quasi-monochromatic (Carr and Reyes 1999). The instantaneous sources (density or acceleration microstructures?) should accordingly have a parallel extent of a few kilometers and spread a few hundred kilometers along the radio emitting field line. The discrete nature of S-bursts is not yet understood: their pulsed character could be due to sporadic electron injection or to the time evolution of the resonant process leading to radio emission generation (see Zarka 1998).

S-burst occurrence is higher when Io is magnetically connected to regions of intense surface field, and it is anti-correlated to the brightness of the UV and IR spots (Genova and Calvert 1988, Connerney *et al.* 1993). Zarka *et al.* (1996) suggested that depending on the amplitude of the surface field, a variable fraction of precipitated electrons is lost through collisions and heating of the ionosphere – producing UV and IR emissions – while the rest is adiabatically mirrored back with a loss-cone distribution allowing it to generate radio emission through the cyclotron-maser mechanism. This could explain the anti-correlation of "optical" and radio outputs, as well as the negative frequency drift of S-bursts (produced by upward moving electrons). When the IFT foot moves through negative surface field gradients, detrapping of electrons should also enhance the loss-cone distribution and increase the radio emission intensity.

(4) The absence of solar wind control of Io-DAM is consistent with the fact that Io is embedded in the inner jovian magnetosphere and thus "insulated" from external conditions. Zarka *et al.* (2001b) has computed the power dissipated in the Io–Jupiter interaction by estimating the energy flux incident on the obstacle cross section. The dominant incident power is provided by the rotating plasma trapped in the jovian magnetic field and convected across Io's ionosphere, the primary energy source being of course Jupiter's rotation. It may be noted that a total dissipated power of $\sim 2 \times 10^{12}$ W implies an increase of the jovian rotation period at a rate of $\sim 6 \times 10^{-19}$ s/s (2×10^{-11} second per year) and a corresponding increase of Io's orbital radius of 0.5 mm per year. Finally, let us recall that the most accurate determination of Jupiter's rotation period was obtained from long-term (~24 years) observations of the Io-DAM occurrence (Higgins *et al.* 1997).

Energetics of Electromagnetic Emissions at Io's Footprint

Multi-wavelength observations of the Io footprints have placed strong constraints on the power delivered by precipitation of energetic particles. Emitted power reaches ~3–10×10^{10} W in the IR, $\sim 5 \times 10^{10}$ W in the UV, and a total of 10^{9-10} W in radio waves (Zarka *et al.* 1997, Bhardwaj *et al.* 2001). The total electromagnetic power, $\sim 10^{11}$ W, is thus remarkably large (equivalent to the Earth's total auroral power) concentrated in a $\sim 60 \times 200$ km^2 area. IR and UV emissions require precipitated power of $\sim 3 \times 10^{11}$ W in the form of 10–100 keV electrons, while the cyclotron-maser mechanism (which produces the radio emission), with an efficiency about 1%, implies a precipitating power of 10^{11-12} W in the 1–10 keV range. This is consistent with the $\sim 10^{12}$ W per hemisphere dissipated in the Io–Jupiter interaction, provided that the electron energy is distributed in the appropriate energy ranges. Crary (1997), in the only attempt to compute electron precipitations triggered by Io, suggested that electron energization results from Fermi acceleration by the parallel electric field associated with Alfvén waves. His prediction of a total electron power $\sim 10^{11}$ W with an average (maximum) energy of 78(500) keV, and a power $\sim 10^9$ W in the 1–10 keV range, does not fulfill the above requirements, especially in the radio range.

As mentioned above, in situ measurements in Io's wake (I0 flyby) by *Galileo* EPD and PLS revealed bi-directional electron beams with energies in the range ~0.1 to ~200 keV and power of a few 10^{10} W (Williams *et al.* 1999, Frank and Paterson 1999). Such beams could in principle provide enough power for the footprint electromagnetic emissions if they extend to sufficiently high magnetic latitudes, but their relation with the footprint emissions has been ques-

tioned (Mauk *et al.* 2001). The question of the acceleration process thus remains open. Bi-directional beams may result from upwards acceleration near the ionosphere by an Earth-like auroral potential structure, followed by mirroring. Chust *et al.* (2001) proposed a two-step energization process taking advantage of the mass-loading electric field followed by Landau acceleration of electrons by low-frequency plasma waves (possibly excited by Alfvén currents). Very intense ULF electromagnetic waves detected by *Galileo*/PWS in the southern Alfvén wing bring support to this class of scenarios, still to be developed quantitatively.

22.5 UNRESOLVED QUESTIONS

One of the major unresolved questions involves Io's far-field plasma interaction. How does the coupling mechanism between Io and Jupiter's ionosphere function? There is even a lack in our knowledge about the magnetospheric properties such as plasma densities, and electron and ion temperatures at higher latitudes. The mechanism that accelerates the electrons necessary to excite Io's footprint is also not known. The origin of the bi-directional electron beams in the wake of Io is not understood. Other transport processes along the field lines, such as mass transport, i.e., via slow-mode waves have not been studied in enough detail.

Mass loading at Io is also a subject that deserves more attention. The canonical value for the total mass rate is $1\,\mathrm{ton\,s^{-1}}$ (Broadfoot *et al.* 1979) derived from *Voyager* observations. This number might undergo temporal variations and should be confirmed by further analysis. It is currently not clear how this mass rate is supplied to Io's torus. Most mass leaves Io as neutrals (Shemansky 1980). Bagenal (1997) estimated only 20–50% is locally ionized at Io while Saur *et al.* (2003) reduced the limit to <20%. An important mechanism for the neutral mass loss could be sputtering by torus ions (Johnson 1990, Smyth 1998). Modeling of the sputtering is a difficult task since the region around Io's exosphere needs to be treated appropriately. Neither collision-free models nor fluid models can be applied.

A model of Io's multi-ion chemistry that self-consistently includes the plasma physics in three dimensions has not yet been undertaken and will lead to important new results. The current models are at one extreme self-consistent 3-D one-fluid MHD models (e.g., Linker *et al.* (1998) or Combi *et al.* (1998)) or one-fluid ion chemistry models (e.g., Summers and Strobel 1996). The models by Saur *et al.* (1999, 2002) are partly self-consistent, 3-D, and two-fluid, where the electrons energetics are treated accurately.

The feedback mechanisms of Io's atmosphere and the plasma interaction is relatively poorly understood, too. The plasma interaction modifies the general structure (e.g., Saur *et al.* 2002) as well as for example, the temperature of the atmosphere (e.g., Strobel *et al.* 1994), while in turn a modified neutral atmosphere will affect the plasma interaction.

Acknowledgements. We appreciate that Jon Linker provided us with Figure 22.10 and 22.8. We thank Christer Neimök for going out of his way to prepare Figure 22.2. We also appreciate helpful comments by the reviewers.

REFERENCES

Acuña, M. H., F. M. Neubauer, and N. F. Ness, Standing Alfvén wave current system at Io: *Voyager 1* observations, *J. Geophys. Res.* **86**, 8513–8521, 1981.

Bagenal, F., Alfvén wave propagation in the Io plasma torus, *J. Geophys. Res.* **88**, 3013–3025, 1983.

Bagenal, F., The ionization source near Io from *Galileo* wake data, *Geophys. Res. Lett.* **24**, 2111–2114, 1997.

Bagenal, F. and Y. Leblanc, Io's Alfvén wave pattern and the jovian decametric arcs, *Astron. & Astrophys.* **197**, 311–319, 1988.

Banks, P. M. and G. Kockarts, *Aeronomy*, vol. A, Academic Press, 1973a.

Banks, P. M. and G. Kockarts, *Aeronomy*, vol. B, Academic Press, 1973b.

Baumjohann, W. and R. A. Treumann, *Basic Space Plasma Physics*, 1996.

Belcher, J. W., The low-energy plasma in the jovian magnetosphere, in *Physics of the Jovian Magnetosphere*, A. J. Dessler, ed., pp. 68–105, Cambridge University Press, 1983.

Belcher, J. W., C. K. Goertz, J. D. Sullivan, and M. H. Acuna, Plasma observations of the Alfvén wave generated by Io, *J. Geophys. Res.* **86**, 8508–8512, 1981.

Bhardwaj, A., G. R. Gladstone, and P. Zarka, An overview of Io flux tube footprints in Jupiter's auroral ionosphere, *Adv. Space Res.* **27**, 1915–1922, 2001.

Bigg, E. K., Influence of the satellite Io on Jupiter's decametric emission, *Nature* **203**, 1008–1010, 1964.

Bridge, H. S. *et al.*, Plasma observations near Jupiter: Initial results from *Voyager 1*, *Science* **204**, 987–991, 1979.

Broadfoot, A. L., M. J. S. Belton, P. Z. Takacs, B. R. Sandel, D. E. Shemansky, J. B. Holberg, J. M. Ajello, S. K. Atreya, T. M. Donahue, H. W. Moos, J. L. Bertaux, J. E. Blamont, D. F. Strobel, J. C. McConnell, A. Dalgarno, R. Goody, and M. B. McElroy, Extreme ultraviolet observations from *Voyager 1.* encounter with Jupiter, *Science* **204**, 979–982, 1979.

Brown, R. A. and F. H. Chaffee, High-resolution spectra of sodium emission from Io, *AJ* **187**, L125–L126, 1974.

Brown, R. A., C. B. Pilcher, and D. F. Strobel, Spectrophotometric studies of the Io torus, in *Physics of the Jovian Magnetosphere*, A. J. Dessler, pp. 197–225, Cambridge University Press, 1983.

Carr, T. D. and F. Reyes, Microstructure of jovian decametric S bursts, *J. Geophys. Res.* **104**, 25 127–25 141, 1999.

Carr, T. D., M. D. Desch, and J. K. Alexander, Phenomenology of magnetospheric radio emissions, in *Physics of the Jovian Magnetosphere*, A. J. Dessler, pp. 226–284, Cambridge University Press, 1983.

Chen, F. F., *Introduction to Plasma Physics and Controlled Fusion*, 2nd edn., 1984.

Chust, T., A. Roux, W. S. Kurth, and D. A. Gurnett, Electron acceleration by plasma waves in the Io flux tube, *Eos* **82**, 2001.

Clarke, J. T., J. Ajello, G. E. Ballester, L. B. Jaffel, J. E. P. Connerney, J.-C. Gérard, G. R. Gladstone, D. Grodent, W. Pryor, J. Trauger, and J. H. Waite, Ultaviolet emissions from the magnetic footprints of Io, Ganymede and Europa on Jupiter, *Nature* **415**, 997–1000, 2002.

Clarke *et al.*, J. T., Far-UV imaging of Jupiter's aurora with HST WFPC 2, *Science* **274**, 404–409, 1996.

Cloutier, P. A., R. E. Daniell Jr., A. J. Dessler, and T. W. Hill, A

cometary ionosphere model for Io, *Astrophys. Space Sci.* **55**, 93–112, 1978.

Combi, M. R., K. Kabin, T. I. Gombosi, D. L. De Zeeuw, and K. G. Powell, Io's plasma environment during the *Galileo* flyby: Global three-dimensional MHD modeling with adaptive mesh refinement, *J. Geophys. Res.* **103**, 9071–9081, 1998.

Connerney, J., Doing more with Jupiter's magnetic field, in *Planetary Radio Emissions III*, H. O. Rucker and S. J. Bauer, eds, pp. 13–33, Austrian Academy of Science, 1992.

Connerney, J. E. P., Magnetic fields of the outer planets, *J. Geophys. Res.* **98**, 18 659–18 679, 1993.

Connerney, J. E. P. and T. Satoh, The H_3^+ ion: A remote diagnostic of the jovian magnetosphere, *Phil. Trans. Roy. Soc. A.* **358**, 2471, 2000.

Connerney, J. E. P., R. Baron, T. Satoh, and T. Owen, Images of excited H_3^+ at the foot of the Io flux tube in Jupiter's atmosphere, *Science* **262**, 1035–1038, 1993.

Connerney, J. E. P., M. H. Acuna, N. F. Ness, and T. Satoh, New models of Jupiter's magnetic field constrained by the Io flux tube footprint, *J. Geophys. Res.* **103**, 11 929–11 939, 1998.

Crary, F. J., On the generation of an electron beam by Io, *J. Geophys. Res.* **102**, 37–49, 1997.

Crary, F. J. and F. Bagenal, Coupling the plasma interaction at Io to Jupiter, *Geophys. Res. Lett.* **24**, 2135–2138, 1997.

Delamere, P. A., F. Bagenal, R. E. Ergun, and Y.-J. Su, Momentum transfer between the Io plasma wake and Jupiter's ionosphere, *J. Geophys. Res.* **108**, 2003.

Dessler, A. J. and J. W. Chamberlain, jovian longitudinal asymmetry in Io-related and Europa-related auroral hot spots, *ApJ* **230**, 974–981, 1979.

Dessler, A. J. and T. W. Hill, Jovian longitudinal control of Io-related radio emissions, *ApJ* **227**, 664–675, 1979.

Drell, S. D., H. M. Foley, and M. A. Ruderman, Drag and propulsion of large satellites in the ionosphere: An Alfvén propulsion engine in space, *J. Geophys. Res.* **70**, 3131–3145, 1965.

Ellis, G. R. A., Observations of the Jupiter S bursts between 3.2 and 32 MHz, *Aust. J. Phys.* **35**, 165–175, 1982.

Erkaev, N. V., V. S. Semenov, V. A. Shaidurov, D. Langmayr, H. K. Biernat, and H. O. Rucker, Investigation of MHD slow shocks propagating along the Io flux tube, *Internat. J. Geomag. Aeron.* **3**, 67–76, 2002.

Frank, L. A. and W. R. Paterson, Production of hydrogen ions at Io, *J. Geophys. Res.* **104**, 10 345–10 354, 1999.

Frank, L. A. and W. R. Paterson, Return to Io by the *Galileo* spacecraft: Plasma observations, *J. Geophys. Res.* **105**, 25 363–25 378, 2000.

Frank, L. A. and W. R. Paterson, Passage through Io's inonospheric plasmas by the *Galileo* spacecraft, *J. Geophys. Res.* **106**, 26 209–26 224, 2001.

Frank, L. A. and W. R. Paterson, Plasma observed with the *Galileo* spacecraft during its flyby over Io's northern polar region, *J. Geophys. Res.* **107**, 1029, 2002.

Frank, L. A., W. R. Paterson, K. L. Ackerson, V. M. Vasyliunas, F. V. Coroniti, and S. J. Bolton, Plasma observations at Io with the *Galileo* spacecraft, *Science* **274**, 394–395, 1996.

Geissler, P. E., A. S. McEwen, W. Ip, M. J. S. Belton, T. V. Johnson, W. H. Smyth, and A. P. Ingersoll, *Galileo* imaging of atmospheric emissions from Io, *Science* **285**, 870–874, 1999.

Geissler, P. E., W. H. Smyth, A. S. McEwen, W. Ip, M. J. S. Belton, T. V. Johnson, A. P. Ingersoll, K. Rages, W. Hubbard, and A. J. Dessler, Morphology and time variability of Io's visible aurora, *J. Geophys. Res.* **106**, 26 137–26 146, 2001.

Genova, F. and M. G. Aubier, Io-dependent sources of the jovian decameter emission, *Astron. & Astrophys.* **150**, 139–150, 1985.

Genova, F. and W. Calvert, The source location of jovian millisecond radio bursts with respect to Jupiter's magnetic field, *J. Geophys. Res.* **93**, 979–986, 1988.

Genova, F., P. Zarka, and C. H. Barrow, *Voyager* and Nançay observations of the jovian radio emission at different frequencies: Solar wind effect and source extent, *Astron. & Astrophys.* **182**, 159–162, 1987.

Goertz, C. K., Io's interaction with the plasma torus, *J. Geophys. Res.* **85**, 2949–2956, 1980.

Goertz, C. K. and P. A. Deift, Io's interaction with the magnetosphere, *Planet. Space Sci.* **21**, 1399–1415, 1973.

Goldreich, P. and D. Lynden-Bell, Io, a jovian unipolar inductor, *ApJ* **156**, 59–78, 1969.

Goldstein, M. L. and C. K. Goertz, Theories of radio emissions and plasma waves, in *Physics of the Jovian Magnetosphere*, A. J. Dessler, pp. 317–352, Cambridge University Press, 1983.

Green, J., The Parker challenge, *Eos* **81**, 200, 2000.

Gurnett, D. A. and C. K. Goertz, Multiple Alfvén wave reflections excited by Io: Origin of the jovian decametric arcs, *J. Geophys. Res.* **86**, 717–722, 1981.

Gurnett, D. A., W. S. Kurth, A. Roux, S. J. Bolton, and C. F. Kennel, *Galileo* plasma wave observations in the Io plasma torus and near Io, *Science* **274**, 391–392, 1996.

Gurnett, D. A., A. Persoon, W. Kurth, A. Roux, and S. Bolton, Electron densities near Io from *Galileo* plasma wave observations, *J. Geophys. Res.* **106**, 26 225–26 232, 2001a.

Gurnett, D. A. *et al.*, An overview of *Galileo* plasma wave observations during the I31 and I32 flybys of Io, *Eos* **87**, 2001b.

Higgins, C. A., T. D. Carr, F. Reyes, W. B. Greenman, and R. G. Lebo, A redefinition of Jupiter's rotation period, *J. Geophys. Res.* **102**, 22 033–22 041, 1997.

Hill, T. W. and D. H. Pontius, Plasma injection near Io, *J. Geophys. Res.* **103**, 19 879–19 885, 1998.

Hill, T. W. and V. M. Vasyliūnas, Jovian auroral signature of Io's corotational wake, *J. Geophys. Res.* **107**, 1464, doi:10.1029/2002JA009,514, 2002.

Hill, T. W., A. J. Dessler, and C. K. Goertz, Magnetospheric models, in *Physics of the Jovian Magnetosphere*, A. J. Dessler, pp. 353–394, Cambridge University Press, 1983.

Hinson, D. P., A. J. Kliore, F. M. Flasar, J. D. Twicken, P. J. Schindler, and R. G. Herrera, *Galileo* radio occultation measurements of Io's ionosphere and plasma wake, *J. Geophys. Res.* **103**, 29 343, 1998.

Hospodarsky, G. B. *et al.*, Control of jovian radio emissions by the Galilean moons as observed by *Cassini* and *Galileo*, in *Planetary Radio Emissions V*, H. O. Rucker and S. J. Baver, eds, pp. 155–164, Austrian Academy of Science, 2001.

Huddleston, D. E., R. J. Strangeway, J. Warnecke, C. T. Russell, M. G. Kivelson, and F. Bagenal, Ion cyclotron waves in the Io torus during the *Galileo* encounter: Warm plasma dispersion analysis, *Geophys. Res. Lett.* **24**, 2143–2146, 1997.

Huddleston, D. E., R. J. Strangeway, J. Warnecke, C. T. Russell, and M. G. Kivelson, Ion cyclotron waves in the Io torus: Wave dispersion, free energy analysis, and SO_2^+ source rate estimates, *J. Geophys. Res.* **103**, 19 887–19 899, 1998.

Jeffrey, A. and T. Taniuti, *Non-Linear Wave Propagation*, Academic Press, 1964.

Johnson, R. E., *Energetic Charged-Particle Interactions with Atmospheres and Surfaces*, Springer-Verlag, 1990.

Kaiser, M. L., P. Zarka, W. S. Kurth, G. B. Hospodarsky, and D. A. Gurnett, *Cassini* and *Wind* stereoscopic observations of jovian non-thermal radio emissions: Measurements of beamwidths, *J. Geophys. Res.* **105**, 16 053–16 062, 2000.

Khurana, K. K., M. G. Kivelson, and C. T. Russell, Interaction of Io with its torus: Does Io have an internal magnetic field?, *Geophys. Res. Lett.* **24**, 2391–2394, 1997.

Kivelson, M. G., K. K. Khurana, R. J. Walker, C. T. Russell, J. A. Linker, D. J. Southwood, and C. Polanskey, A magnetic signature at Io: Initial report from the *Galileo* magnetometer, *Science* **273**, 337–340, 1996a.

Kivelson, M. G., K. K. Khurana, R. J. Walker, J. Warnecke, C. T. Russell, J. A. Linker, D. J. Southwood, and C. Polanskey, Io's interaction with the plasma torus: *Galileo* magnetometer report, *Science* **274**, 396–398, 1996b.

Kivelson, M. G., K. K. Khurana, C. T. Russell, M. V. Volwerk, S. P. Joy, M. Volwerk, R. J. Walker, C. Z. Zimmer, and J. A. Linker, Magnetized or unmagnetized: Ambiguity persits following *Galileo*'s encounters with Io in 1999 and 2000, *J. Geophys. Res.* **106**, 26 121–26 135, 2001a.

Kivelson, M. G., K. K. Khurana, C. T. Russell, and R. J. Walker, Magnetic signature of a polar pass over Io, *Eos* **82**, 2001b.

Kliore, A. J., G. Fjeldbo, B. L. Seidel, D. N. Sweetnam, T. T. Sesplaukis, P. M. Woiceshyn, and S. I. Rasool, The atmosphere of Io from *Pioneer 10* radio occultation measurement, *Icarus* **24**, 407–410, 1975.

Kopp, A., Modifications of the electrodynamic interaction between Jupiter and Io due to mass loading effects, *J. Geophys. Res.* **101**, 24 943–24 954, 1996.

Kupo, I., Y. Mekler, and A. Eviatar, Detection of ionized sulphur in the jovian magnetosphere, *Astrophys. J.* **205**, L51–L54, 1976.

Lecacheux, A., M. Y. Boudjada, H. O. Rucker, J. L. Bougeret, R. Manning, and M. L. Kaiser, Jovian decameter emissions observed by the *Wind* waves radioastronomy experiment, *Astron. & Astrophys.* **329**, 776–784, 1998.

Lellouch, E., M. J. S. Belton, I. de Pater, S. Gulkis, and T. Encrenaz, Io's atmosphere from microwave detection of SO_2, *Nature* **346**, 639–641, 1990.

LeQuéau, D., Planetary radio emissions from high magnetic latitudes: The "Cyclotron-Maser" theory, in *Planetary Radio Emissions II*, H. O. Rucker and S. J. Baver, eds, pp. 381–398, Austrian Academy of Science, 1988.

Linker, J. A. and M. A. McGrath, Modeling ultraviolet emission near Io, *Eos* **79**, 1998.

Linker, J. A., M. G. Kivelson, and R. J. Walker, An MHD simulation of plasma flow past Io: Alfvén and slow mode perturbations, *Geophys. Res. Lett.* **15**, 1311–1314, 1988.

Linker, J. A., M. G. Kivelson, and R. J. Walker, The effect of mass loading on the temperature of a flowing plasma, *Geophys. Res. Lett.* **16**, 763–766, 1989.

Linker, J. A., M. G. Kivelson, and R. J. Walker, A three-dimensional MHD simulation of plasma flow past Io, *J. Geophys. Res.* **96**, 21 037–21 053, 1991.

Linker, J. A., K. K. Khurana, M. G. Kivelson, and R. J. Walker, MHD simulations of Io's interaction with the plasma torus, *J. Geophys. Res.* **103**, 19 867–19 877, 1998.

Linker, J. A., R. Lionello, M. G. Kivelson, and R. J. Walker, MHD models of Io's interaction with the plasma torus: Comparison with the polar flybys, *Eos* **82**, 2001.

Mauk, B. H., D. J. Williams, and A. Eviatar, Understanding Io's space environment interaction: Recent energetic electron measurements from *Galileo*, *J. Geophys. Res.* **106**, 26 195–26 208, 2001.

Morabito, L. A., S. P. Synnott, P. N. Kupferman, and S. A. Collins, Discovery of currently active extraterrestrial volcanism, *Science* **204**, 972, 1979.

Ness, N. F., M. H. Acuña, R. P. Lepping, L. F. Burlaga, K. W. Behannon, and F. M. Neubauer, Magnetic field studies at Jupiter by *Voyager 1*: Preliminary results, *Science* **204**, 982–987, 1979.

Neubauer, F. M., Nonlinear standing Alfvén wave current system at Io: Theory, *J. Geophys. Res.* **85**, 1171–1178, 1980.

Neubauer, F. M., Comment on "Interaction of Io with its torus: Does Io have an internal magnetic field?" by K. K. Khurana, M. G. Kivelson and C.T. Russell, *Geophys. Res. Lett.* **25**, 2349, 1998a.

Neubauer, F. M., The sub-Alfvénic interaction of the Galilean satellites with the jovian magnetosphere, *J. Geophys. Res.* **103**, 19 843–19 866, 1998b.

Neubauer, F. M., Alfvén wings and electromagnetic induction in the interiors: Europa and Callisto, *J. Geophys. Res.* **104**, 28 671, 1999.

Neubauer, F. M., On the plasma distribution in the polar regions of the Galilean satellites, particularly Io: Field-aligned plasma motion, *Eos* **48**, F787, 2000.

Oliversen, R. J., F. Scherb, W. H. Smyth, M. E. Freed, R. C. Woodward, M. L. Marconi, K. D. Retherford, O. L. Lupie, and J. P. Morgenthaler, Sunlit Io atmospheric [O I] 6300 A emission and the plasma torus, *J. Geophys. Res.* **106**, 26 183–26 194, 2001.

Parker, E. N., The alternative paradigm for magnetospheric physics, *J. Geophys. Res.* **101**, 10 587–10 625, 1996.

Peale, S. J., P. Cassen, and R. T. Reynolds, Melting of Io by tidal dissipation, *Science* **203**, 892–894, 1979.

Pearl, J., R. Hanel, V. Kunde, W. Maguire, K. Fox, S. Gupta, C. Ponnamperuma, and F. Raulin, Identification of gaseous SO_2 and new upper limits for other gases on Io, *Nature* **280**, 755–758, 1979.

Piddington, J. H. and J. F. Drake, Electrodynamic effects of Jupiter's satellite Io, *Nature* **217**, 935–937, 1968.

Prangé, R., D. Rego, D. Southwood, P. Zarka, S. Miller, and W.-H. Ip, Rapid energy dissipation and variability of the Io–Jupiter electrodynamic circuit, *Nature* **379**, 323–325, 1996.

Queinnec, J. and P. Zarka, Io-controlled decameter arcs and Io–Jupiter interaction, *J. Geophys. Res.* **103**, 26 649–26 666, 1998.

Queinnec, J. and P. Zarka, Flux, power, energy and polarization of jovian S-bursts, *Planet. Space Sci.* **49**, 365–376, 2001.

Retherford, K. D., H. W. Moos, D. F. Strobel, and B. C. Wolven, Io's equatorial spots: Morphology of neutral UV emissions, *J. Geophys. Res.* **105**, 27 157–27 165, 2000.

Roesler, F. L., H. W. Moos, R. J. Oliversen, R. C. Woodward, K. D. Retherford, F. Scherb, M. A. McGrath, W. H. Smyth, P. D. Feldman, and D. F. Strobel, Far-ultraviolet imaging spectroscopy of Io's atmosphere with HST/STIS, *Science* **283**, 353–357, 1999.

Russell, C. T. and M. G. Kivelson, Detection of SO in Io's exosphere, *Science* **287**, 1998, 2000.

Satoh, T. and J. E. P. Connerney, Jupiter's H_3^+ emissions viewed in corrected jovimagnetic coordinates, *Icarus* **141**, 236–252, 1999.

Satoh, T., J. E. P. Connerney, and R. Baron, Emission source model of Jupiter's H_3^+ aurorae: A generalized inverse analysis of images, *Icarus* **122**, 1–23, 1996.

Saur, J., *Plasma Interaction of Io and Europa with the Jovian Magnetosphere*, Dissertation, Institut für Geophysik und Meteorologie der Universität zu Köln, 2000.

Saur, J., D. F. Strobel, F. M. Neuabuer, and M. E. Summers, Possible generation mechanism for observed oxygen glow patterns in Io's atmosphere, *Eos* **82**, 1998.

Saur, J., F. M. Neubauer, D. F. Strobel, and M. E. Summers, Three-dimensional plasma simulation of Io's interaction with the Io plasma torus: Asymmetric plasma flow, *J. Geophys. Res.* **104**, 25 105–25 126, 1999.

Saur, J., F. M. Neubauer, D. F. Strobel, and M. E. Summers, Io's ultraviolet aurora: Remote sensing of Io's interaction, *Geophys. Res. Lett.* **27**, 2893–2896, 2000.

Saur, J., F. M. Neubauer, D. F. Strobel, and M. E. Summers, Interpretation of *Galileo*'s Io plasma and field observations: The J0, I24, I27 flybys, and close polar passes, *J. Geophys. Res.* p. 1422, 2002.

Saur, J., D. Strobel, F. Neubauer, and M. Summers, The ion mass loading rate at Io, *Icarus* **163**, 456–468, 2003.

Schunk, R. W., Transport equations for aeronomy, *Planet. Space Sci.* **23**, 437–485, 1975.

Shemansky, D. E., Mass-loading and diffusion-loss rates of the Io plasma torus, *ApJ* **242**, 1266–1277, 1980.

Smith, B. A., E. M. Shoemaker, S. W. Kieffer, and A. F. Cook, The role of SO_2 in volcanism on Io, *Nature* **280**, 738–743, 1979.

Smyth, W. H., Energy escape rate of neutrals from Io and the implications for local magnetospheric interactions, *J. Geophys. Res.* **103**, 1998.

Southwood, D. J. and M. W. Dunlop, Mass pickup in sub-Alfvénic plasma flow: A case study for Io, *Planet. Space Sci.* **32**, 1079–1086, 1984.

Southwood, D. J., M. G. Kivelson, R. J. Walker, and J. A. Slavin, Io and its plasma environment, *J. Geophys. Res.* **85**, 5959–5968, 1980.

Strobel, D. F. and B. C. Wolven, The atmosphere of Io: Abundance and sources of sulfur dioxide and atomic hydrogen, *Astrophys. Space Sci.* **277**, 271–287, 2001.

Strobel, D. F., X. Zhu, and M. E. Summers, On the vertical thermal structure of Io's atmosphere, *Icarus* **111**, 18–30, 1994.

Strobel, D. F., J. Saur, F. M. Neuabuer, and M. E. Summers, Modeling Io's electrodynamic interaction with its torus: Comparsion with recent observations, *Eos* **82**, 2001.

Su, Y., R. Ergun, F. Bagenal, and P. Delamare, Io-related jovian auroral arcs: Modeling parallel electric fields, *J. Geophys. Res.* **108**, 1094, 2002.

Summers, M. E. and D. F. Strobel, Photochemistry and vertical transport in Io's atmosphere and ionosphere, *Icarus* **120**, 290–316, 1996.

Szegö, K., K. Glassmeier, R. Bingham, A. Bogdanov, C. Fischer, G. Haerendel, A. Brinca, T. Cravens, E. Dubinin, K. Sauer, L. Fisk, T. Gombosi, N. Schwadron, P. Isenberg, M. Lee, C. Mazelle, E. Möbius, U. Motschmann, V. D. Shapiro, B. Tsurutani, and G. Zank, Physics of mass loaded plasmas, *Space Sci. Rev.* **94**, 429–671, 2000.

Thorne, R. M., J. W. D, L. D. Zhang, and S. Stone, Energetic electron butterfly distributions near Io, *J. Geophys. Res.* **104**, 14 755–14 766, 1999.

Vasavada, A. R., A. H. Bouchez, A. P. Ingersoll, B. Little, C. D. Anger, and the *Galileo* SSI team, Jupiter's visible aurora and Io footprint, *J. Geophys. Res.* **104**, 27 133, 1999.

Warnecke, J., M. G. Kivelson, K. K. Khurana, D. E. Huddleston, and C. T. Russell, Ion cyclotron waves observed at *Galileo*'s Io encounter: Implications for neutral cloud distribution and plasma composition, *Geophys. Res. Lett.* **24**, 2139–2142, 1997.

Williams, D. J., B. H. Mauk, R. E. McEntire, E. C. Roelof, T. P. Armstrong, B. Wilken, J. G. Roederer, S. M. Krimigis, T. A. Fritz, and L. J. Lanzerotti, Electron beams and ion composition measured at Io and in its torus, *Science* **274**, 401–403, 1996.

Williams, D. J., R. M. Thorne, and B. Mauk, Energetic electron beams and trapped electrons at Io, *J. Geophys. Res.* **104**, 14 739–14 753, 1999.

Wolf-Gladrow, D. A., F. M. Neubauer, and M. Lussem, Io's interaction with the plasma torus: A self-consistent model, *J. Geophys. Res.* **92**, 9949–9961, 1987.

Wright, A. N., The interaction of Io's Alfvén waves with the jovian magnetosphere, *J. Geophys. Res.* **92**, 9963–9970, 1987.

Zarka, P., Auroral radio emissions at the outer planets: Observations and theories, *J. Geophys. Res.* **103**, 20 159–20 194, 1998.

Zarka, P., T. Farges, B. P. Ryabov, M. Abada-Simon, and L. Denis, A scenario for jovian S-bursts, *Geophys. Res. Lett.* **23**, 125–128, 1996.

Zarka, P., B. P. Ryabov, V. B. Ryabov, R. Prangé, M. Abada-Simon, T. Farges, and L. Denis, On the origin of jovian decameter radio bursts, in *Planetary Radio Emissions IV*, H. O. Rucker and S. J. Baver, eds, pp. 51–63, Austrian Academy of Science, 1997.

Zarka, P., J. Queinnec, and F. Crary, Low-frequency limit of jovian radio emissions and implications on source locations and Io plasma wake, *Planet. Space Sci.* **49**, 1137–1149, 2001.

Zarka, P., R. A. Treumann, B. P. Ryabov, and V. B. Ryabov, Magnetically-driven planetary radio emissions and applications to extrasolar planets, *Astrophys. Space Sci.* **277**, 293–300, 2001b.

Zarka, P., D. Langmayr, A. Gerbault, L. Denis, A. Coffre, and F. Korver, Lead angle of Io-controlled radio emission: Alfvén wave or slow shock?, in *Magnetospheres of the Outer Planets*, 2002.